

# THE PHYSICS OF GALAXY CLUSTERING I: A MODEL FOR SUBHALO POPULATIONS

ANDREW R. ZENTNER<sup>1</sup>, ANDREAS A. BERLIND<sup>3</sup>, JAMES S. BULLOCK<sup>4,5,6</sup>,  
 ANDREY V. KRAVTSOV<sup>1,2</sup>, AND RISA H. WECHSLER<sup>1,2,6,7</sup>  
 The Astrophysical Journal, submitted

## ABSTRACT

We present a semi-analytic model for Cold Dark Matter halo substructure that can be used as a framework for studying the physics of galaxy formation and as an ingredient in halo models of galaxy clustering. The model has the following main ingredients: (1) extended Press-Schechter mass accretion histories; (2) host halo density profiles computed according to the trends observed in cosmological simulations; (3) distributions of initial orbital parameters of accreting subhalos measured in a high-resolution simulation of three Milky Way-size halos; and (4) integration of the orbital evolution of subhalos including the effects of dynamical friction and tidal mass loss. We perform a comprehensive comparison of the model calculations to the results of a suite of high-resolution cosmological simulations. The comparisons show that subhalo statistics, such as the velocity and mass functions, the radial distributions, and the halo occupation distributions agree well over three orders of magnitude in host halo mass and at various redshifts. We find that both in the simulations and in our model the radial distributions of subhalos are significantly shallower than that of the dark matter density. The abundance of subhalos in a host is set by competition between tidal disruption and new accretion. Halos of high mass and halos at high redshift tend to host more subhalos because the subhalos have, on average, been accreted more recently. Similarly, at a fixed mass and epoch, halos that formed more recently host a larger number of subhalos. Observed “fossil groups” may represent an extreme tail of this correlation. We find a related correlation between host halo concentration and satellite abundance at fixed host mass,  $N_{\text{sat}} \propto c_{\text{vir}}^{-a}$ , where  $a$  changes with redshift and host-to-subhalo mass ratio. Lastly, we use our substructure model to populate host halos in one of the high-resolution cosmological simulations, replacing the actual subhalos resolved in this simulation and using the host mass as the only input for the model calculation. We show that the resulting correlation function of such a hybrid halo ensemble is indistinguishable from that measured directly in the simulation. This supports one of the key tenets of the standard halo model — the assumption that the halo occupation distribution is statistically independent of the host halo environment.

*Subject headings:* cosmology: theory, galaxies: formation, large-scale structure of universe

## 1. INTRODUCTION

Numerical simulations of structure formation set within the cold dark matter (CDM) paradigm (see White & Rees 1978; Blumenthal et al. 1984) have revealed that virialized, dark matter halos are rife with distinct, self-bound substructure or *subhalos* (e.g. Moore et al. 1999; Klypin et al. 1999a,b; Ghigna et al. 1998, 2000; Kravtsov, Gnedin, & Klypin 2004; Diemand, Moore, & Stadel 2004; Gao et al. 2004a; Reed et al. 2004). It is tempting to associate subhalos, particularly large subhalos, with galaxies in groups and clusters (Klypin et al. 1999a; Kravtsov & Klypin 1999; Colín et al. 1999; Moore et al. 1999). Lending support to this conjecture, Kravtsov et al. (2004) used natural assumptions to connect galaxy luminosity to subhalos and showed that the clustering properties of sub-

halos and their *host* halos match the observed clustering properties of galaxies (see also Neyrinck et al. 2004). This implies that the occupation distribution of subhalos must be quite similar to the occupation distribution of galaxies in host halos (e.g. Berlind & Weinberg 2002) and that luminous satellite galaxies are likely associated with massive dark matter subhalos. A corollary of this is that if one understands the physical processes that govern subhalo occupation, one gains significant insight into the physics of galaxy clustering.

The abundances of subhalos within host dark matter halos are determined through the interplay of several important and relatively distinct physical processes. If one imagines, for simplicity, the development of a subhalo population as a sequence, the first process to consider is the merging of halos to form ever larger systems. In the prevailing CDM paradigm of hierarchical structure growth, halo merger rates are governed by the initial density field and the global cosmological model, and tend to be more rapid at early times. The second step is to consider the evolution of merged subhalos in the potential of the host halo. In contrast to merger statistics, subhalo evolution is influenced by local processes in the high-density environment of the host, like dynamical friction, tidal mass loss, and heating by violent interactions with other structures. These processes reduce the amount of distinct substructure within host systems over timescales of order the local dynamical time. At early times, when the merger timescale is short compared to the dynamical time, we ex-

<sup>1</sup> Kavli Institute for Cosmological Physics and Department of Astronomy and Astrophysics, The University of Chicago, Chicago, IL 60637, USA; zentner,risa@kicp.uchicago.edu, andrey@oddjob.uchicago.edu

<sup>2</sup> The Enrico Fermi Institute, The University of Chicago, Chicago, IL 60637, USA

<sup>3</sup> Center for Cosmology and Particle Physics and Department of Physics, New York University, New York, NY 10003, USA; aberlind@cosmo.nyu.edu

<sup>4</sup> Harvard-Smithsonian Center for Astrophysics, Cambridge, MA 12138, USA; jbullock@cfa.harvard.edu

<sup>5</sup> Department of Physics and Astronomy, The University of California at Irvine, Irvine, CA 92697, USA

<sup>6</sup> Hubble Fellow

<sup>7</sup> Enrico Fermi Fellow

pect high substructure counts within individual host halos. At late times, we expect substructure to be reduced, as subhalos are packed into more and more dense environments inside larger and larger host systems. All of these physical processes are purely gravitational, but have a significant effect on the small-scale clustering of subhalos. By implication, galaxy clustering statistics are governed by these processes as well.

This paper is the first of a series of studies of the physical processes that govern galaxy clustering statistics. In the context of this series, this paper represents a description of our theoretical methodology, but the content of this paper is considerably more general. We present a semi-analytic model that can be used to make predictions for the substructure populations of dark matter halos. The model begins with the computation of the merger histories of dark matter halos and approximates the subsequent effects of dynamical friction and tidal mass after accretion. In the regime where they are commensurable, we make detailed comparisons of this model to the results of high-resolution  $N$ -body simulations to assess the accuracy and applicability of the model (see § 4). We emphasize that the model we present in this first paper includes only the effect of gravity and neglects any effects of baryon cooling and condensation. Our strategy in so doing is to build upon a tractable model that can be robustly be tested with  $N$ -body simulations in a variety of ways. In this way, the importance of additional processes and approximations can be ascertained in a well-controlled way and we will pursue these aims in the subsequent papers of this series.

There are advantages to using an analytic model that has been tested against existing simulations in a wide range of applications. First, an analytic model can quickly generate a statistically-large number of realizations of subhalo populations within host halos of various masses with a relatively small computational effort. As a result, such a model can complement direct simulation where limited dynamic range severely restricts the size of any host halo sample in a study of halo substructure. Along these lines, Islam, Taylor, and Silk (2003) used a semi-analytic approach to study a population of black holes, which may exist as remnants of the first stars, in the Milky Way (MW) halo. This study would have required a dynamic range that is unachievable even with dissipationless numerical simulations. In addition, such a model can be used to study the effects of non-standard cosmological inputs on subhalo populations over a wide range of parameter space. Zentner & Bullock (2003, ZB03 hereafter) used such an approach to estimate the influence of modifications to the primordial power spectrum on the populations of satellite halos and the prospects for using satellite halo populations to constrain cosmology.

More closely tied to the specific aims of the papers in this series, analytic substructure models can provide an important ingredient for modeling the large-scale clustering of galaxies by predicting halo occupation distributions. Coupled with a relatively low-resolution, large-volume simulation, such a model can be used to calculate galaxy clustering statistics, including environmental dependences, in a way that explicitly accounts for complicated non-linear effects such as the bias of host halos with respect to the dark matter (Mo & White 1996; Jing 1998; Sheth, Mo,

& Tormen 1999; Seljak & Warren 2004). Alternatively, a subhalo model can be utilized in conjunction with an analytic halo model (see, e.g. Seljak 2000; Scoccimarro et al. 2001) to make analytic predictions for clustering statistics rapidly, for a wide range of the space of cosmological parameters and for various assumptions about galaxy formation. We demonstrate this utilization explicitly in § 4.6. Importantly, when used in these ways, our subhalo model provides a framework for rapidly testing hypotheses about the physics of galaxy formation against the observed clustering properties of galaxies. Of equal importance, the results of the semi-analytic model predictions are easy to dissect and understand in a physical way. We explore these avenues in the subsequent papers of this series.

The outline of this paper is as follows. In § 2, we briefly describe three sets of  $N$ -body simulations that we use to test our analytic subhalo model over a broad range of host halo properties. In § 3, we describe all of the ingredients of the substructure model. The model is an extension of the work of ZB03 and we pay particular attention to differences and improvements upon that work. As we discuss below, our model is similar in many respects to the model developed by Taylor & Babul (2001, 2004a), and shares common ingredients with the models of Benson et al. (2002), Oguri & Lee (2004), and van den Bosch, Tormen, & Giocoli (2004b). We present our results and compare them to the results of high-resolution numerical simulations in § 4. In this section, we also discuss our results in the context of many recent observational and theoretical developments and more generally describe the utility of our substructure model. We draw conclusions in § 5. In a forthcoming companion paper (A. A. Berlind et al., in preparation), we use this model to address the origin of the nearly power-law galaxy correlation function and several other features of galaxy clustering statistics.

Throughout this paper we refer to self-bound subunits that are within the virial radius of another, larger halo as *subhalos* or *satellites*. We refer to halos that are not contained within another, larger halo, and therefore are not classified as subhalos, as *host* halos. We use the term *halo* to refer to both host halos and satellite halos.

## 2. NUMERICAL SIMULATIONS

The logic behind our use of numerical simulations is as follows. By their nature, semi-analytic models attempt to model complicated, non-linear dynamical processes using simple prescriptions and rely on inputs distilled from numerical simulations. Some of the inputs for the evolution of subhalos is provided by controlled (non-cosmological) simulations (e.g., Colpi, Mayer, & Governato 1999; Velázquez & White 1999; Taylor & Babul 2001; Mayer et al. 2002; Hashimoto et al. 2003; Taffoni et al. 2003; Kazantzidis et al. 2004b). However, cosmological simulations are still needed to specify the initial orbital parameters of accreted subhalos and the structure of cosmological halos. We assume halo density profiles derived from cosmological simulations for a wide range of masses and cosmologies as described below. We determine the initial orbital parameters of subhalos from a high-resolution simulation of three nearly MW-size halos. We subsequently compare the results of our model with the subhalos in simulations of a very high resolution cluster-size halo and a

large number of halos in a cosmological simulation with uniform mass resolution and a different power spectrum normalization. These comparisons over a wide range of halo masses and different power spectrum normalizations are thus non-trivial tests of the applicability of our model.

In both our simulations and our semi-analytic modeling, we quantify the size of host dark matter halos by their virial masses  $M_{\text{vir}}$  or, equivalently, their virial radii  $R_{\text{vir}}$ . We define the halo virial radius as the radius within which the mean density is equal to the virial overdensity  $\Delta_{\text{vir}}$ , multiplied by the mean matter density of the universe  $\rho_M$ , so that  $M_{\text{vir}} = 4\pi\rho_M\Delta_{\text{vir}}R_{\text{vir}}^3/3$ . For the simulated halos, this radius is centered on the particle with the highest local density. The quantity  $\Delta_{\text{vir}}$  can be estimated from the spherical top-hat collapse approximation (Eke, Navarro, & Frenk 1998). We compute  $\Delta_{\text{vir}}$  using the fitting function provided by Bryan & Norman (1998). In the  $\Lambda$ CDM cosmology that we consider,  $\Delta_{\text{vir}}(z=0) \simeq 337$  and tends toward the standard CDM (i.e.  $\Omega_M = 1$ ) value  $\Delta_{\text{vir}} \rightarrow 178$  at high redshift ( $z \gtrsim 1$ ).

All of our simulations were performed with the Adaptive Refinement Tree (ART)  $N$ -body code (see Kravtsov, Klypin, & Khokhlov 1997; Kravtsov 1999). The simulated Galaxy-size halos are the three halos discussed in detail in Klypin et al. (2001, hereafter K01) and Kravtsov, Gnedin, & Klypin (2004, hereafter KGK04). Briefly, K01 used the ART code to model the evolution of three MW-size halos in a standard “concordance,” flat,  $\Lambda$ CDM cosmology with  $\Omega_M = 1 - \Omega_\Lambda = 0.3$ ,  $h = 0.7$ , and  $\sigma_8 = 0.9$  in a comoving box of size  $25 h^{-1}\text{Mpc}$  on a side. The simulation began with a uniform  $256^3$  grid covering the entire computational volume. Higher force resolution was achieved about collapsing structures by recursive refinement of all such regions using an adaptive refinement algorithm. The grid cells were refined if the particle mass contained within them exceeded a certain specified threshold value.

The multiple mass resolution technique was used to set up the initial conditions. A Lagrangian region corresponding to two virial radii about each halo was resampled with the highest resolution particles of mass  $m_p = 1.2 \times 10^6 h^{-1}\text{M}_\odot$ , corresponding to  $1024^3$  particles in the box, at the initial timestep,  $z_i = 50$ . The high mass resolution region was surrounded by layers of particles of increasing mass with a total of five particle species. Only the regions containing the highest-resolution particles were adaptively refined. The maximum level of refinement in the simulations corresponded to a peak formal spatial resolution of approximately  $100h^{-1}\text{pc}$ . The three MW-size halos, referred to as  $G_1$ ,  $G_2$ , and  $G_3$  in KGK04, have virial masses of  $1.13 \times 10^{12} h^{-1}\text{M}_\odot$ ,  $1.14 \times 10^{12} h^{-1}\text{M}_\odot$ , and  $1.45 \times 10^{12} h^{-1}\text{M}_\odot$  respectively, and each of them is resolved with approximately  $\sim 10^6$  highest-resolution particles within their virial radii. Further details can be found in K01 and KGK04.

In addition to these three MW-size halos, we compare our model results to the results of a high-resolution simulation of a cluster-size halo of virial mass  $\sim 1.7 \times 10^{14} h^{-1}\text{M}_\odot$ . The cluster was simulated in a comoving box of  $80 h^{-1}\text{Mpc}$  on a side using the same multiple mass resolution technique described above in the same concordance  $\Lambda$ CDM cosmology, as described in Tasitsiomi et al. (2004). The peak formal resolution was

$0.6 h^{-1}\text{kpc}$  and the mass of the highest resolution particles was  $m_p = 3.95 \times 10^7 h^{-1}\text{M}_\odot$ . The cluster was resolved with  $\approx 4.4 \times 10^6$  particles within its virial radius. This high-resolution simulated cluster halo was referred to as CL2 HR by Tasitsiomi et al. (2004).

Lastly, we compare our model predictions to the subhalo populations in a cosmological simulation with uniform mass resolution containing a large number of host halos over a wide range of masses. This simulation followed the evolution of  $512^3$  particles in an  $80 h^{-1}\text{Mpc}$  comoving box, corresponding to a particle mass of  $m_p = 3.16 \times 10^8 h^{-1}\text{M}_\odot$ . The cosmological model was the same  $\Lambda$ CDM cosmology as above, but with a “low” power spectrum normalization of  $\sigma_8 = 0.75$ . The peak formal spatial resolution of the simulation was  $1.2h^{-1}\text{kpc}$  comoving. At  $z = 0$  the simulation box contains  $\approx 1.2 \times 10^5$  host halos with  $M_{\text{vir}} > 10^{11} h^{-1}\text{M}_\odot$  and  $\approx 3 \times 10^4$  subhalos with a bound mass  $> 10^{11} h^{-1}\text{M}_\odot$ . We use this simulated halo and subhalo population to perform a comprehensive test of our model. This simulation was described in Kravtsov et al. (2004), where the simulation was referred to as  $\Lambda\text{CDM}_{80}$ .

In all three of the numerical simulations described above, halos and subhalos were identified using a variant of the Bound Density Maxima Algorithm (Klypin et al. 1999b). The first steps of the halo-finding algorithm are to compute the local overdensity at each particle position using a smoothing kernel of 24 particles and to find the locations of local maxima in the density field. Starting with the highest density particle and proceeding toward lower density, each density peak is marked as a potential halo center and then surrounded by a sphere of fixed radius  $r_{\text{find}}$ . All particles within  $r_{\text{find}}$  are excluded from further consideration as potential halo centers. The search radius parameter  $r_{\text{find}}$  is set according to the size of the smallest object that we aim to identify. For the simulated MW-size halos this was set to  $r_{\text{find}} = 10h^{-1}\text{kpc}$ , while for the high-resolution cluster simulation and the  $\Lambda\text{CDM}_{80}$  simulation we set  $r_{\text{find}} = 50h^{-1}\text{kpc}$ . After identifying potential halo centers, we analyze the surrounding particles and iteratively remove particles that are unbound (see Klypin et al. 1999b). All remaining bound particles are then used to compute halo/subhalo properties such as mass  $M$ , the circular velocity profile  $V_{\text{circ}}(r) = \sqrt{GM(< r)/r}$ , and the peak circular velocity  $V_{\text{max}}$ .

For subhalos, the outer boundary or outer radius of the system can be somewhat ambiguous and dependent upon a particular definition. Our convention is to adopt a truncation radius  $r_t$  for subhalos, at which the logarithmic slope of the density profile constructed from the bound particles becomes greater than a critical value of  $d\ln(\rho)/d\ln r = -0.5$ . The iterative removal of unbound particles is imperfect, and for subhalos some fraction of unbound particles with nearly constant density is left on the outskirts of the subhalo. Some of these particles are from the diffuse mass of the background host halo and often some are unbound particles from the tidal debris of the subhalo itself. Generally, the density profiles of the tidally-truncated subhalos have an outer slope steeper than  $d\ln(\rho)/d\ln r = -3$  until the radius where the density of background particles becomes comparable to the density of the residual background particles not removed

by the unbinding procedure. At this radius, the profile flattens significantly and this is the radius that we identify as the subhalo truncation radius. The above criterion is thus based on the fact that we do not expect the density profiles of CDM halos to be shallower than this and, empirically, this definition of truncation radius is approximately equivalent to the radius at which the density of the bound particles is equal to the background host halo density. We note that the outer profiles of subhalos generally fall off with  $d \ln(\rho)/d \ln r < -3$ , so the bound mass converges well before the truncation radius is reached. Consequently, any uncertainty in the truncation radius does not translate into an appreciable error in the bound mass of the subhalo. However, throughout most of this work, we quantify the size of satellite halos by their maximum circular velocities  $V_{\max}$ , because this quantity is measured more robustly and is not subject to the same ambiguity as a particular mass definition. This makes our results easier to compare to the results of other researchers using different subhalo identification algorithms and mass definitions.

### 3. A MODEL FOR HALO SUBSTRUCTURE

In order to determine the substructure properties of a dark matter halo we must model its mass accretion history as well as the orbital evolution of all accreted subhalos once they are incorporated into the host system. We model substructure using a semi-analytic technique that incorporates simplifying approximations and empirical relations observed in numerical simulations. The model is an updated and improved version of the model described in ZB03 and in Koushiappas, Zentner, & Walker (2004) and draws on the earlier work of Bullock, Kravtsov, & Weinberg (2000, 2001a). The model of ZB03 and the improved model that we describe here are similar in many respects to the models developed by Taylor & Babul (2001, 2004a), Benson et al. (2002), Oguri & Lee (2004), and van den Bosch et al. (2004b). In this section, we give a brief description of the specific model that we use, highlighting additions and improvements. We begin with a brief review of the generation of merger histories followed by a discussion of our assumptions about the density profiles of CDM halos and subhalos. We conclude this section with a description of our initial conditions for subhalo orbits and our treatment of subhalo dynamics within the host potential.

#### 3.1. Merger Trees

The first step in determining the properties of halo substructure is to model the mass accretion history of the host dark matter halo. A *merger tree* that approximates many of the results of  $N$ -body simulations can be constructed from the linear power spectrum of density perturbations using a statistical Monte Carlo technique based on the extended Press-Schechter (EPS) formalism (Bond et al. 1991; Lacey & Cole 1993, hereafter LC93; Lacey & Cole 1994). Using this method, we generate a list of the masses and accretion redshifts of all subhalos that have merged to form a host halo of a given mass at a given redshift. In this way we are able to track both diffuse mass and subhalo accretion via mergers for each host. By generating a large number of such merger trees, we can attempt to sample the diverse mass accretion histories that result in

a host halo of a given fixed mass at the time at which we are interested in “observing” the halo (most often,  $z = 0$ ).

Several authors have explored implementations of specific variations of the EPS formalism to construct realistic merger trees (e.g. LC93; Sheth & Lemson 1999; Cole et al. 2000). We employ the particular algorithm advocated by Somerville & Kolatt (1999), which conserves mass explicitly. Let  $\sigma(M)$  represent the *rms* fluctuation amplitude in the density field smoothed on a scale  $R$  such that the mean mass contained within a sphere of radius  $R$  is  $M$ , that is  $M = 4\pi\rho_M R^3/3$  where  $\rho_M$  is the mean mass density of the Universe. Following the notation established in LC93, let us denote  $S(M) \equiv \sigma^2(M)$ ,  $\Delta S \equiv S(M) - S(M + \Delta M)$ ,  $w(t) \equiv \delta_c(t)$ , and  $\delta w = w(t) - w(t + \Delta t)$ , where  $\delta_c(t)$  is the linear overdensity for collapse at time  $t$  in our choice of cosmological model ( $\delta_c \approx 1.68$ , see LC93; White 1996). With these definitions, the probability that a halo of mass  $M$  at time  $t$  accretes an amount of mass associated with a change  $\Delta S$  in a timestep corresponding to  $\delta w$  is given by

$$P(\Delta S, \delta w) d(\Delta S) = \frac{\delta w}{\sqrt{2\pi}(\Delta S)^{3/2}} \exp \frac{-(\delta w)^2}{2\Delta S} d(\Delta S). \quad (1)$$

Following Somerville & Kolatt (1999), we generate merger histories by starting at the redshift that we wish to observe the final halo (usually  $z = 0$ ) and step backward in time. At each timestep, we select halo progenitors by drawing values of  $\Delta M$  from the distribution of Equation (1). In this way, we generate a list of progenitor masses and accretion redshifts at each time step. If the minimum halo mass that we wish to track is  $M_{\min}$ , then in order to reproduce the conditional mass function of EPS theory we must choose a timestep such that  $\delta w = \sqrt{f_{ts} M_{\min} dS(M_{\min})/dM}$  with  $f_{ts} \ll 1$ . In practice, we choose  $f_{ts} = 10^{-2}$  as an adequate compromise between accuracy and computation time. We retain all information about mergers with  $\Delta M \geq M_{\min}$  and treat events with  $\Delta M < M_{\min}$  as diffuse mass accretion. In what follows, we employ several different values of  $M_{\min}$ , depending upon the minimum halo size that we wish to track in each case.

#### 3.2. Halo Mass Density Profiles

After accretion, each subhalo is subject to various dynamical processes as it orbits within the host halo. The amount of mass that remains bound to the subhalo and whether or not the subhalo survives as a distinct, self-bound system depend upon the density structure of both the subhalo and the host halo. In this subsection we describe our assumptions about the mass density profiles of CDM halos.

We characterize the size of host halos by their virial masses  $M_{\text{vir}}$  and virial radii  $R_{\text{vir}}$ , as described in § 2. In the interest of simplicity, we model all halos with the spherically-averaged density profile of Navarro, Frenk, & White (1997, NFW hereafter):

$$\rho(r) = \rho_s \left( c_{\text{vir}} \frac{r}{R_{\text{vir}}} \right)^{-1} \left( 1 + c_{\text{vir}} \frac{r}{R_{\text{vir}}} \right)^{-2}, \quad (2)$$

where  $c_{\text{vir}}$  is the concentration parameter, which describes the scale radius  $r_s \equiv R_{\text{vir}}/c_{\text{vir}}$ , where the logarithmic slope

of the profile,  $d \ln \rho / d \ln r = -2$ . The normalization is fixed by the requirement that the mass interior to  $R_{\text{vir}}$  be equal to  $M_{\text{vir}}$ . The NFW profile can be rewritten as a circular velocity profile  $V_{\text{circ}}^2(r) = V_{\text{vir}}^2 c_{\text{vir}} g(x) / x g(c_{\text{vir}})$ , where  $x \equiv r/r_s$ , the function  $g(y) \equiv \ln(1+y) - y/(1+y)$ , and  $V_{\text{vir}} \equiv \sqrt{GM_{\text{vir}}/R_{\text{vir}}}$  is the halo virial velocity. The maximum of the circular velocity profile occurs at a radius  $r_{\text{max}} \simeq 2.16 r_s$ , at a value of  $V_{\text{max}}^2 \simeq 0.22 V_{\text{vir}}^2 c_{\text{vir}} / g(c_{\text{vir}})$ .

The concentrations of dark matter halos observed in simulations are tightly correlated with their mass accretion histories (Wechsler et al. 2002, hereafter W02; Zhao et al. 2003). We account for the correlation between the concentrations of host halos and their mass accretion histories using the proposal of W02. Specifically, we assign to each host halo a *collapse epoch*  $a_c$ , by fitting the mass accretion history of the halo, computed as described above in § 3.1, with the functional form

$$M_{\text{vir}}(a) = M_{\text{vir}}(a_0) \exp(-2a_c[a_0/a - 1]), \quad (3)$$

where  $a_0$  is the scale factor at which we observe the halo to have mass  $M_{\text{vir}}(a_0)$ . From the fitted value of  $a_c$ , we assign each halo a concentration through

$$c_{\text{vir}} = 5.125 \left( \frac{a_0}{a_c} \right). \quad (4)$$

The mass accretion histories of the subhalos are generally more poorly sampled than the accretion histories of hosts because subhalos have significantly smaller masses than their hosts and are built by correspondingly fewer mergers above  $M_{\text{min}}$ . It is possible to sample the merger trees of halos and smaller subhalos roughly uniformly by lowering the value of  $M_{\text{min}}$  for the smaller subhalos but this leads to a rapid increase in the computational expense of generating the merger trees and entails calculating mergers with halos that are far less massive than any halos that we expect to host luminous galaxies. Instead, we assign concentrations to subhalos in the following way. If the subhalo mass is greater than  $10^3 M_{\text{min}}$ , then we nearly always have a well-sampled mass accretion history with  $\gtrsim 50$  merger events and we use the procedure of W02 as outlined above. Otherwise, we use the analytic model of Bullock et al. (2001b, B01 hereafter) to compute the mean concentration for the mass of each subhalo at the time of accretion. We then compute the actual value of  $c_{\text{vir}}$  that we assign to each subhalo by selecting randomly from a log-normal probability distribution for  $c_{\text{vir}}$  with standard deviation  $\sigma(\log(c_{\text{vir}})) = 0.14$ . B01 and W02 determined this to be a good approximation for the statistical scatter of  $c_{\text{vir}}$  for halos of fixed virial mass in their simulations.

### 3.3. Orbital Evolution of Subhalos

With the accretion histories and the density profiles of the host and all accreted subhalos in place, the next step is to track the orbital evolution of each accreted system to determine how severely each satellite halo is affected by dynamical friction and tidal mass loss.

The first step in tracking the subhalo evolution is to assign the initial parameters of the subhalo orbit. Upon accretion onto the host, each subhalo is assigned an initial orbital energy based on the range of binding energies observed in numerical simulations. We use the simulations of

the MW-like halos  $G_1$ ,  $G_2$ , and  $G_3$  (K01; KGK04) to determine the initial orbital parameters for subhalos at each accretion event. For each accretion event, we located the timestep in the simulation at which the most bound particle in the subhalo first appeared within the virial radius of the main host. We then measured the orbital energy and angular momentum of the infalling subhalo. Note that because outputs of only 96 epochs were saved for the simulation, each infalling subhalo does not have exactly the same relation to the host halo at the time that we measure these parameters and this may contribute some degree of uncertainty to the initial conditions. As in the previous work of Klypin et al. (1999a) and Bullock et al. (2000), we find that the initial energy distribution of orbits can be well-described by placing each satellite on an initial orbit with an energy equal to the orbital energy of a *circular* orbit of radius  $R_{\text{circ}} = \eta R_{\text{vir}}$ , where  $R_{\text{vir}}$  is the virial radius of the host halo at the time of accretion, and  $\eta$  is drawn from a uniform distribution on the interval  $[0.6, 1.0]$ .

It is very important to describe the angular momenta of satellite orbits correctly in order to estimate the degree to which the subhalos are affected by tidal mass loss because mass loss is most rapid at pericenter, leading to a very strong preference for subhalos on highly eccentric orbits to be disrupted by tides (for examples, see Taylor & Babul 2001, 2004a). We parameterize the initial angular momenta of subhalos with the orbital circularity  $\epsilon$ , defined as the angular momentum in units of the angular momentum of a circular orbit of the same energy,  $\epsilon \equiv J/J_{\text{circ}}$ . The circularity parameter is clearly restricted to the interval  $0 \leq \epsilon \leq 1$ . In Figure 1, we show the measured distribution of  $\epsilon$  from the mergers experienced by  $G_1$ ,  $G_2$ , and  $G_3$  in terms of the fraction of in-falling satellites with a given initial circularity,  $df_{\text{sat}}(\epsilon)/d\epsilon$ . We find the distribution of orbital circularities to be well-fit by a one-parameter  $\beta$ -distribution,

$$\frac{df_{\text{sat}}(\epsilon)}{d\epsilon} = \frac{\Gamma(2a)}{\Gamma^2(a)} \epsilon^{a-1} (1-\epsilon)^{a-1}, \quad (5)$$

which is valid on the interval  $0 \leq \epsilon \leq 1$  and has the simple properties of the mean  $\langle \epsilon \rangle = 1/2$ , and standard deviation  $\sigma(\epsilon) = 1/2\sqrt{2a+1}$ . Our best fit of  $a = 2.22$  is shown as the solid line in Fig. 1. The distribution of Eq. 5 matches the measured mean  $\langle \epsilon \rangle_{\text{sim}} \simeq 0.495$  and standard deviation  $\sigma_{\text{sim}}(\epsilon) \simeq 0.219$  ( $\sigma_{\text{fit}}(\epsilon) \simeq 0.214$ ) of subhalo orbital circularities in the simulation quite well. As we were completing our work, a study of the initial orbits of satellite halos was published by Benson (2004), the results of which appear to be in approximate agreement with our findings.

The distributions of initial orbits that we have described were culled from simulations of three MW-size halos and may not be generic. However, over the subhalo mass range that we are able to probe, we detect no statistically-significant variation in the input distributions with mass. Additionally, we observe no significant evolution of these distributions with redshift. An example of this last point is shown in Fig. 1, where the open squares represent the circularity distribution measured for the subhalos with the earliest 25% of accretion epochs. The agreement with the full distribution is apparent. We proceed by assuming that we can set initial conditions by drawing randomly from the energy and angular momentum distributions that we have

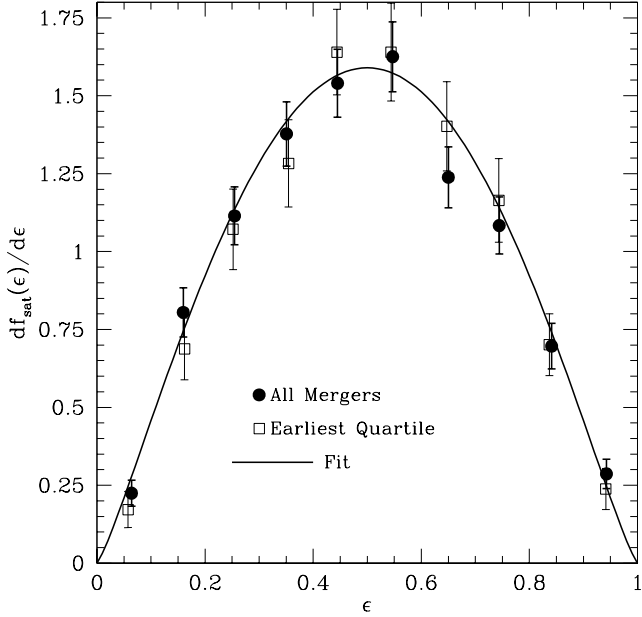


FIG. 1.— Input orbital circularity distribution for infalling subhalos measured from the high-resolution simulations of the  $G_1$ ,  $G_2$ , and  $G_3$  MW-size halos discussed in KGK04. The *filled circles* show the measured distribution for all merging subhalos at the time of accretion. The *open squares* represent the distribution measured from only the earliest 25% of all mergers. The *solid line* shows a fit of the distribution of all mergers to the  $\beta$ -distribution given by Equation (5) with  $a = 2.22$  (see main text for details).

described for *all* merging satellites of *all* masses at *all* redshifts. The comparisons with simulations discussed below show that this assumption appears to be reasonable.

We evolve the orbits of satellites by treating them as point particles under the influence of the spherical, NFW potential of the host halo with an added force term to approximate the effect of dynamical friction. As in ZB03, we account for dynamical friction by using a modified form of the Chandrasekhar formula (Chandrasekhar 1943; Binney & Tremaine 1987). The approximations of Chandrasekhar result in a frictional force exerted opposite the velocity of the satellite of magnitude

$$F_{\text{DF}} \simeq \frac{4\pi G^2 M_{\text{sat}}^2 \rho_{\text{host}}(r)}{V_{\text{sat}}^2} \ln(\Lambda) \left( \text{erf}(x) - \frac{2x}{\sqrt{\pi}} \exp(-x^2) \right), \quad (6)$$

where  $r$  is the position of the satellite halo relative to the center of the host potential,  $M_{\text{sat}}$  is the bound mass of the satellite,  $\rho_{\text{host}}(r)$  is the mass density of the host halo at this position,  $V_{\text{sat}}$  is the velocity of the satellite, and  $x \equiv V_{\text{sat}}/\sqrt{2\sigma(r)^2}$ , where  $\sigma(r)^2$  is the one-dimensional velocity dispersion of particles in the host halo. For the NFW host, we estimate the one-dimensional velocity dispersion of the host particles by assuming an isotropic dispersion tensor; a simple fitting formula for  $\sigma(r)$  obtained in this way is given by ZB03. We assign the Coulomb logarithm  $\ln(\Lambda)$ , according to the prescription of Hashimoto, Funato, & Makino (2003), which they found to provide a good match to the results of their  $N$ -body experiments for individual orbits:

$$\ln(\Lambda) = \ln \left( \frac{r}{R_{\text{sat}}} \right) + I(R_{\text{sat}}/r_s), \quad (7)$$

where  $r$  is the radial position of the satellite,  $R_{\text{sat}}$  is the radius of the satellite (which we identify with the truncation radius as described below),  $r_s$  is the scale radius of the NFW profile of the satellite halo, and the function  $I(R_{\text{sat}}/r_s)$  is an integral of the scattering of background particles with impact parameters  $b < R_{\text{sat}}$  over the radial density profile of the subhalo, following the method of White (1976). A convenient fitting function for  $I(R_{\text{sat}}/r_s)$  for NFW profiles is given in ZB03 [see their Eq. (8)].

As in Taylor & Babul (2001) and ZB03, we estimate mass loss due to tidal stripping using a tidal approximation. The first step is to estimate the tidal radius  $r_{\text{tide}}$ , as the radius at which the tidal force from the host balances the attractive force of the satellite halo (e.g. King 1962). At each timestep in the subhalo orbit, we estimate the mass outside of the tidal radius  $M_{\text{sat}}(> r_{\text{tide}})$ , and strip mass on a timescale proportional to the inverse of the angular velocity  $\omega^{-1}$ , of the satellite. Specifically, the change in mass associated with the satellite at each timestep is

$$\delta M_{\text{sat}} = \alpha M_{\text{sat}}(> r_{\text{tide}}) (\delta t / \omega^{-1}). \quad (8)$$

ZB03 motivated the  $\sim \omega^{-1}$  choice of timescale by examining the typical orbital energies of tidally-stripped material in controlled simulations (Johnston 1998). The parameter  $\alpha$  is intended to absorb many of the complicated details of the process of tidal mass loss, which is dependent upon the details of subhalo structure (e.g. Kazantzidis et al. 2004a), and  $\alpha$  is the *only* parameter that we fix in order to normalize the model to simulation results. We choose  $\alpha = 3.5$  as our normalization and discuss this choice further in § 4.1.

Recent controlled  $N$ -body simulations (Hayashi et al. 2003) and the cosmological simulations of the  $G_1$ ,  $G_2$ , and  $G_3$  halos (KGK04) indicate that as mass is lost from a satellite not only is mass from outside of the tidal radius removed, but there is a significant amount of mass redistribution within the tidal radius. Hayashi et al. (2003) and KGK04 find that, on average, the maximum circular velocity of the stripped subhalos varies with bound mass in a remarkably simple way, namely  $V_{\text{max}} \propto M_{\text{sat}}^{\gamma}$ , with  $\gamma \sim 1/4 - 1/3$  and this scaling has been confirmed in the experiments of Kazantzidis et al. (2004b, S. Kazantzidis, private communication) with much higher resolution. We attempt to take approximate account of this redistribution by enforcing the empirical scaling relation  $V_{\text{max}} \propto M_{\text{sat}}^{1/3}$ . For each subhalo, tidal mass loss is most dramatic at each pericenter pass. At each subsequent apocenter pass, we rescale the density profile of the subhalo by scaling  $V_{\text{max}} \propto M_{\text{sat}}^{1/3}$  and set a new scale radius according to the relationship between  $V_{\text{max}}$  and  $r_s$  for field halos provided by the model of B01. As mass is lost, we assume that the shape of the profile maintains the NFW form [Eq. (2)] with a truncation radius  $R_{\text{sat}}$  that we set equal to the radius that contains the remaining bound mass, rather than the tidal radius, which does not vary monotonically.

As the final ingredients to our semi-analytic treatment of halo substructure, we impose criteria for declaring subhalos to be either completely tidally disrupted or centrally

merged with the host halo, and therefore no longer identifiable as distinct substructure. We consider a subhalo completely tidally disrupted if, after any episode of tidal mass loss, the remaining bound mass of the satellite is less than the mass contained within its scale radius,  $M_{\text{sat}}(< r_s)$ . We declare a subhalo centrally merged with its host halo if the apocenter of the subhalo orbit becomes smaller than  $r_{\text{merge}} = 5 \text{ kpc}$  due to dynamical friction. This is a rather conservative central merger criterion, and in practice it is rarely important in our model because subhalos are always severely affected by tides long before their apocentric distances fall below  $r_{\text{merge}}$ , so that they drop out of any mass or  $V_{\text{max}}$  cut that is designed to select subhalos that may potentially host luminous galaxies. The purpose of this criterion is mostly one of pragmatism, to eliminate the integration of very tightly bound orbits which require very small time steps.

### 3.4. The Subhalos of Subhalos

When each subhalo merges with a larger host, the subhalo itself may be the host of still smaller satellite halos. These *subhalos-of-subhalos* (*SOShalos*) can be an important contribution to the total subhalo population, especially in the case of a very massive host halo, such as when a halo typical of a small group merges into the halo of a large cluster. All of the interactions of the SOShalos cannot be accounted for in detail without leading to a very rapid increase in the computational expense of the calculation, mitigating the utility of the semi-analytic approach, the *raison d'être* of which is speed and simplicity, and so some simplifying assumptions must be made.

Taylor & Babul (2004a) treat SOShalos using an efficient averaging scheme that is based on the assumption of self-similarity of the subhalo population of the primary host halo and the SOShalo populations of subhalos. At the level of the main host, they determine the mean amount of mass lost by subhalos during their evolution and the fraction of subhalos with a radial position greater than the radius containing this amount mass  $f_s$ . At each merger event, they then strip a fraction  $f_s$  of the SOShalos associated with the incoming subhalo, starting with the most recently acquired SOShalos (i.e. last in, first out), and place them on correlated orbits within the main host. The remaining SOShalos, the fraction  $1 - f_s$  of SOShalos that were earliest acquired by the incoming subhalo, are then considered too tightly bound to be stripped from the subhalo by the main host and are added to the subhalo system.

We adopt an alternative approximation scheme that is more computationally expensive but does not rely upon the assumptions of self-similarity, the “last in first out” stripping of SOShalos, or the computation of a mean fraction of stripped SOShalos. However, we make several independent simplifying assumptions as follows. We treat SOShalos by considering their evolution through three distinct phases punctuated by abrupt transitions. First, before a subhalo is accreted onto a larger host, it plays the role of a host halo and we simply evolve the orbits of any SOShalos as described in § 3.3. Accordingly, SOShalos can be significantly dynamically evolved and can even fall below our minimum mass or  $V_{\text{max}}$  thresholds prior to being acquired by the main host halo. Second, upon accretion of a subhalo onto a host, we treat the SOShalos of the sub-

halo, if they are present and still above the minimum halo mass of interest, by continuing to integrate their orbits within the subhalo potential, neglecting their interactions with the main host halo. Third, we consider the possibility that a SOShalo may be stripped from the subhalo and deposited in the main host. This represents a transition where the dynamics of the SOShalo go from being dominated by the subhalo to being dominated by the main host. During the evolution of the subhalo in the main host, if the tidal radius of the subhalo becomes smaller than the radial position of a SOShalo, we declare the SOShalo to be stripped off of the subhalo. We then remove it from the subhalo, place it in the potential of the main host, and continue integrating its orbit until the final epoch (usually  $z = 0$ ).

When we place a stripped SOShalo within the potential of the main host, we must assign it an orbit that is closely associated with the orbit of the subhalo from which it was stripped. Johnston (1998) found that the typical specific energy of tidally stripped particles is set by the change in the host halo potential on the length scale of the orbiting satellite,  $\Delta E_{\text{ts}} = r_{\text{tide}} d\Phi_{\text{host}}(r)/dr$ . We set the stripped SOShalo on an orbit with specific energy equal to the orbital energy of its *parent subhalo* in the *main host*  $\pm \Delta E_{\text{ts}}$ , with the sign of the shift in orbital energy chosen randomly to correspond to the leading and trailing tails of the tidal debris.

## 4. MODEL RESULTS AND COMPARISONS WITH NUMERICAL SIMULATIONS

In this Section, we present the results of the substructure model described in § 3 along with a comprehensive comparison with the results of high-resolution numerical simulations over the mass range where the two approaches can be compared robustly.

### 4.1. Subhalo Velocity and Mass Functions

As in ZB03, the particular algorithm described in § 3 made use of inputs from numerical simulations and, in particular, was designed to approximately reproduce the cumulative velocity function (CVF)  $N_{\text{sat}}(> V_{\text{max}})$ , of simulated MW-size halos (KGK04). The CVF is defined as the number of subhalos above a given threshold in maximum circular velocity  $V_{\text{max}}$ , as a function of  $V_{\text{max}}$ . Figure 2 shows model predictions for CVFs compared to the results of numerical simulations. In all cases, we refer to subhalo maximum circular velocities  $V_{\text{max}}^{\text{sat}}$ , that are scaled by units of the maximum circular velocity of the host halo  $V_{\text{max}}^{\text{host}}$ , in order to approximately scale out the dependence of the velocity function on the size of the host halo and facilitate the comparison of velocity functions of hosts of various sizes. The solid line in Fig. 2 shows the mean CVF from 100 model realizations of a host halo with virial mass  $M_{\text{host}} = 10^{12.1} h^{-1} M_{\odot}$  in a standard  $\Lambda$ CDM cosmology with  $\Omega_M = 1 - \Omega_\Lambda = 0.3$ ,  $h = 0.7$ , and  $\sigma_8 = 0.9$ . The error bars on this result represent the  $1 - \sigma$  realization-to-realization scatter about the mean value measured from these 100 model realizations. The dotted lines show the measured cumulative velocity functions of the three simulated MW-size halos  $G_1$ ,  $G_2$ , and  $G_3$  introduced in § 2. The dotted lines are truncated at the value of  $V_{\text{max}}^{\text{sat}}$  where

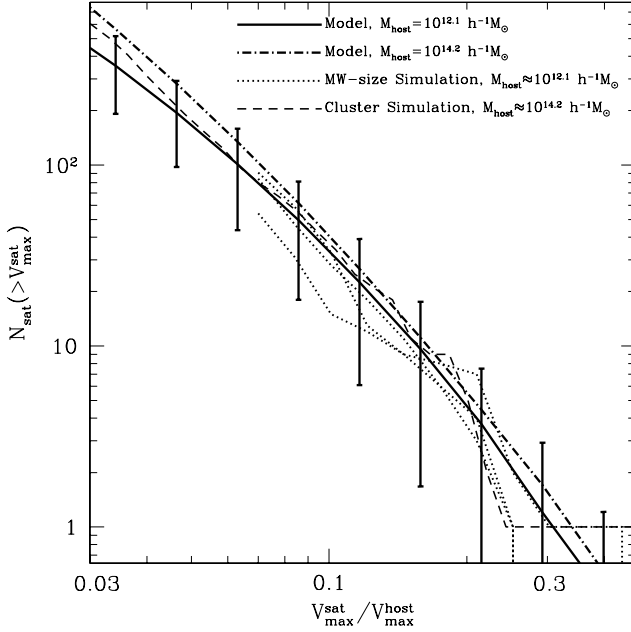


FIG. 2.— The mean cumulative velocity functions  $N_{\text{sat}}(>V_{\text{max}})$ , of satellite halos. The *solid* line depicts the mean value of the number of subhalos with a maximum circular velocity greater than  $V_{\text{max}}^{\text{sat}}$ , as a function of  $V_{\text{max}}^{\text{sat}}$  predicted by 100 model realizations of a  $M_{\text{host}} = 10^{12.1} h^{-1} M_{\odot}$  host halo. Velocities are scaled in units of the maximum circular velocity of the host halo  $V_{\text{max}}^{\text{host}}$ . The errorbars depict the  $1 - \sigma$  scatter among the 100 model realizations. The *dotted* lines show the cumulative velocity functions of the three simulated MW-size halos. The *dashed* line shows the cumulative velocity function of the simulated cluster-size halo (CL2 HR in Tasitsiomi et al. 2004). The *dot-dashed* line is the mean predicted cumulative velocity function from 100 model realizations of a  $M_{\text{host}} = 10^{14.2} h^{-1} M_{\odot}$  halo. In the interest of clarity, the realization-to-realization scatter is not shown for this case but is similar to the scatter for the MW-size model realizations.

the simulation halo catalogs become incomplete due to finite resolution. The good agreement between the model CVF and the CVFs of the simulated MW-size halos is apparent and was achieved by setting the mass loss parameter  $\alpha = 3.5$  in Eq. 8. We emphasize that, as in ZB03, our semi-analytic model was normalized to *this statistic only* and as such, it is now possible to make *predictions* for other statistics, and to diagnose and assess the general applicability of the model by comparing these predictions to the results of numerical simulations.

Figure 2 also shows the first prediction of the semi-analytic model compared to the result of an  $N$ -body simulation. The dot-dashed line shows the CVF of a  $M_{\text{host}} = 10^{14.2} h^{-1} M_{\odot}$  cluster-size host halo in the same “concordance” cosmology. For clarity, the scatter among these realizations is not shown, but it is similar to the scatter on the CVFs of the MW-size halos. The dashed line is the CVF of a simulated cluster-size halo of the same mass. The predictions of the model and the simulation are in good agreement as the simulated halo is well within the  $1 - \sigma$  scatter about the mean CVF of the model. Notice also that the model predicts that the CVF should not scale in a precisely self-similar manner with the size of the host. The model results in a CVF that is slightly higher at higher values of  $V_{\text{max}}^{\text{host}}$ . We return to this point shortly.

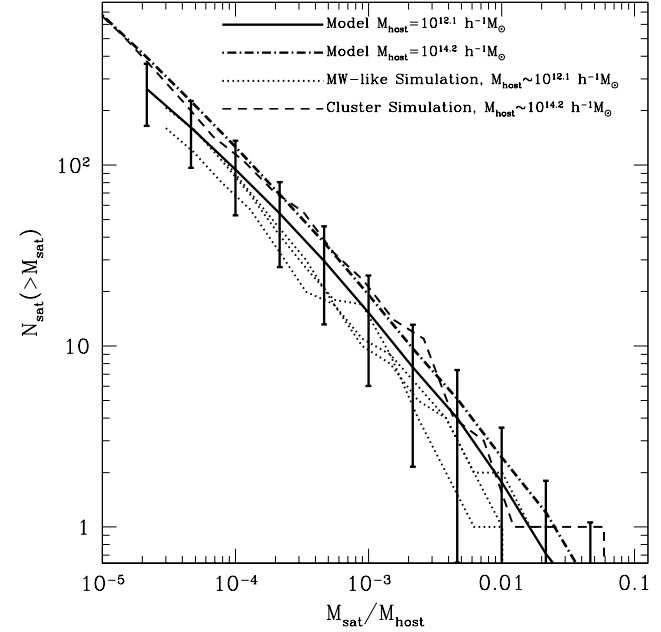


FIG. 3.— The mean cumulative mass function (CMF) of subhalos as a function of subhalo mass relative to the mass of the host halo,  $M_{\text{sat}}/M_{\text{host}}$ . The *solid* line shows the mean value of  $\langle N_{\text{sat}} \rangle (> M_{\text{sat}}/M_{\text{host}})$  for a  $M_{\text{host}} = 10^{12.1} h^{-1} M_{\odot}$  host computed from 100 realizations of the dynamical model of § 3. The errorbars depict the  $1 - \sigma$  scatter among the 100 realizations. The *dotted* lines show the CMFs of the three simulated halos of similar mass described in K01 and KGK04. The *dot-dashed* line shows the mean CMF of a  $M_{\text{host}} = 10^{14.2} h^{-1} M_{\odot}$  halo predicted by 100 model realizations (for clarity, the scatter is not shown in this case but is similar to that of the smaller host). The *dashed* line shows the CMF measured from a high-resolution simulation of a cluster-size halo of a similar mass (halo CL2 HR in Tasitsiomi et al. 2004).

As a further test of our model, we now turn to the cumulative mass function (CMF)  $N_{\text{sat}}(> M_{\text{sat}})$  of subhalos. As with the CVF, we refer to subhalo masses  $M_{\text{sat}}$  in units of the host halo mass  $M_{\text{host}}$  in order to scale out the gross dependence of  $N_{\text{sat}}(> M_{\text{sat}})$  upon the mass of the host halo. We show CMFs in Figure 3. Again, the agreement between the results of the model and the numerical simulations is good, lending confidence in the ability of the model to account approximately for the dominant physical effects that determine subhalo properties, and to be applied more generally. Note also that, just as we saw for the CVF in Fig. 2, the CMFs in Fig. 3 show that the number of subhalos of a given size does not scale self-similarly with the size of the host. Larger host halos tend to have more substructure at a fixed value of  $M_{\text{sat}}/M_{\text{host}}$  (or  $V_{\text{max}}^{\text{sat}}/V_{\text{max}}^{\text{host}}$ ), in agreement with the recent numerical results of Gao et al. (2004a) and the simplified analytic considerations of van den Bosch et al. (2004b).

#### 4.2. The Radial Distribution of Subhalos

The radial distribution of subhalos within their hosts has received a significant amount of attention recently and is a necessary ingredient of models of galaxy clustering statistics (Seljak 2000; Sheth et al. 2001; Berlind & Weinberg 2002) and in the modeling of the flux-ratio anomalies in strong lens systems (e.g., Dalal & Kochanek 2001; Bradač et al. 2002; Chen, Kravtsov, & Keeton 2003). At least

three groups have recently performed convergence studies that demonstrate that the radial distribution of subhalos of all sizes is significantly less centrally-concentrated than the distribution of dark matter (Diemand et al. 2004; Gao et al. 2004a; Nagai & Kravtsov 2005), confirming several earlier results (Ghigna et al. 1998, 2000; Colín et al. 1999; Springel et al. 2001). Diemand et al. (2004) and Gao et al. (2004b) stressed that the observed spatial distribution of galaxies in clusters (Carlberg, Yee, & Ellingson 1997; van der Marel et al. 2000; Lin, Mohr, & Stanford 2004) appears to be more centrally-concentrated and not as strongly anti-biased with respect to the dark matter as the distribution of subhalos in dissipationless  $N$ -body simulations (see also Springel et al. 2001). van den Bosch et al. (2004a) analyzed satellite galaxies in the Two-Degree Field Galaxy Redshift Survey (Colless et al. 2001) finding preliminary indications that observed galaxies do follow a centrally-concentrated, NFW-like radial distribution over a wide range of host halo masses, though they cannot rule out shallower distributions because of incompleteness of close pairs (Cole et al. 2001) and more detailed studies are required to confirm this.

Taylor, Silk, & Babul (2003) and Taylor & Babul (2004b,c) used semi-analytic methods to argue that the distribution of subhalos should be more centrally-concentrated than that observed in simulations and that simulations may still be subject to the problem of “overmerging” in the central regions of halos (see Klypin et al. 1999b). The results of the recent studies by Diemand et al. (2004), Gao et al. (2004a), and Nagai & Kravtsov (2005) cast doubt upon the proposal of Taylor et al. (2003). Nagai & Kravtsov (2005) suggest that the radial distribution of galaxies selected on luminosity cannot be compared directly with that of subhalos selected by mass because galaxies do not likely lose luminosity at the same rate that they lose dark matter while they orbit inside a larger host halo. Nevertheless, it is important to pursue further tests of this issue. The growing importance of the radial distributions of subhalos and various subsets of subhalos with specific properties, coupled with these recent theoretical studies, provide interesting motivations for comparing the spatial distributions of subhalos in our model with that observed in numerical simulations.

In Figure 4, we compare the results of our model predictions for the radial distributions of subhalos with the results of the  $G_1$ ,  $G_2$ , and  $G_3$  MW-size halo simulations and the high-resolution cluster simulation discussed in Tassisomi et al. (2004). In Figure 4, we plot the cumulative number of subhalos at a distance less than  $R$  away from the center of the host halo  $N_{\text{sat}}(< R)$ , as a function of  $R$  and normalize by the total number of subhalos within the virial radius of the halo  $N_{\text{total}}$  (Fig. 2 and Fig. 3 already show that the values of  $N_{\text{total}}$  are in agreement). In the left hand panel, we compare the radial distribution of subhalos within MW-size host halos. We choose the selection criterion  $V_{\text{max}}^{\text{sat}}/V_{\text{max}}^{\text{host}} \geq 0.07$  in order to restrict our results to subhalos that are sufficiently large as to be well-resolved in the simulation and fairly insensitive to numerical effects. The dot-dashed line shows the distribution of dark matter for an NFW profile with a concentration parameter of  $c_{\text{vir}} = 12.6$ . This is a typical value of  $c_{\text{vir}}$  for a MW-size halo in this cosmology (B01) and is the mean value of the

concentration of the 100 hosts in the semi-analytic model. The three simulated MW-size halos  $G_1$ ,  $G_2$ , and  $G_3$  have best-fit concentration parameters of  $c_{\text{vir}} \simeq 9.5$ , 12.5, and 14.5 respectively. Similarly, in the right hand panel of Fig. 4, we compare the radial distribution of subhalos of the simulated cluster halo with the distribution of subhalos in 100 model realizations of a  $M_{\text{host}} = 10^{14.2} h^{-1} M_{\odot}$  host halo. The maximum circular velocity threshold in this case is  $V_{\text{max}}^{\text{sat}}/V_{\text{max}}^{\text{host}} > 0.05$ . Once again, the dot-dashed line represents the distribution of dark matter for an NFW profile with  $c_{\text{vir}} = 6.1$ , which is typical for a halo of this mass and is close to the mean concentration of the 100 hosts in the semi-analytic model. The simulated cluster halo has a best-fitting concentration of  $c_{\text{vir}} = 8.5$ , which is roughly  $\sim 1 - \sigma$  higher than the mean concentration at this mass according to the halo-to-halo scatter observed in simulations (B01). For the simulated subhalo distributions, we computed profiles by stacking the last five simulation outputs ( $a = 1.00, 0.99, 0.98, 0.97, 0.96$  for  $G_1$ ,  $G_2$ , and  $G_3$  and  $a = 1.000, 0.995, 0.990, 0.985, 0.980$  for the cluster) in order to overcome the noise in the measurement.

Several interesting features are evident in Figure 4. First, the anti-bias of the subhalo population with respect to the dark matter is evident in both panels of Fig. 4 for both the simulated halos and the model halos. A MW-size halo typically has  $\sim 35\%$  of its mass within  $\sim 0.2R_{\text{vir}}$ , yet it has only  $\sim 5\%$  of its satellite halos located this close to its center. Second, notice the excellent agreement between the simulation and model subhalo profiles in both panels. Again, this agreement is a non-trivial confirmation of the success and more general applicability of the semi-analytic model. After designing the model to reproduce the *number* of subhalos in a MW-size host, the model naturally recovers the correct radial distribution of satellites within both a MW-size host halo and a more massive cluster-size halo.

The agreement between the model subhalo distribution and the distribution of subhalos in the simulations is an encouraging sign that the semi-analytic model captures the dominant physical processes that determine the demographics of CDM subhalos. Moreover, this indicates that the model of § 3 results in a spatial distribution of subhalos that is in conflict with the model of Taylor et al. (2003) and Taylor & Babul (2004b), who find a much more centrally-concentrated distribution of subhalos. The radial distributions of subhalos in our model support the conclusion that the anti-bias of subhalos with respect to dark matter is a physical effect rather than the result of numerical overmerging, yet it will likely require further study to provide a definitive answer to this question. However, our results indicate that the disagreement between semi-analytic models and simulation results may depend upon the specifics of the model implementation and is not a generic feature of such models.

#### 4.3. The Halo Occupation Distribution of Subhalos

We now turn to a more comprehensive comparison of our semi-analytic model to the predictions of cosmological  $N$ -body simulations. To do this, we compare the results of our model to the subhalo populations in the  $\Lambda\text{CDM}_{80}$  simulation studied by Kravtsov et al. (2004). Recall that the  $\Lambda\text{CDM}_{80}$  simulation was performed for a  $\Lambda\text{CDM}$  cos-

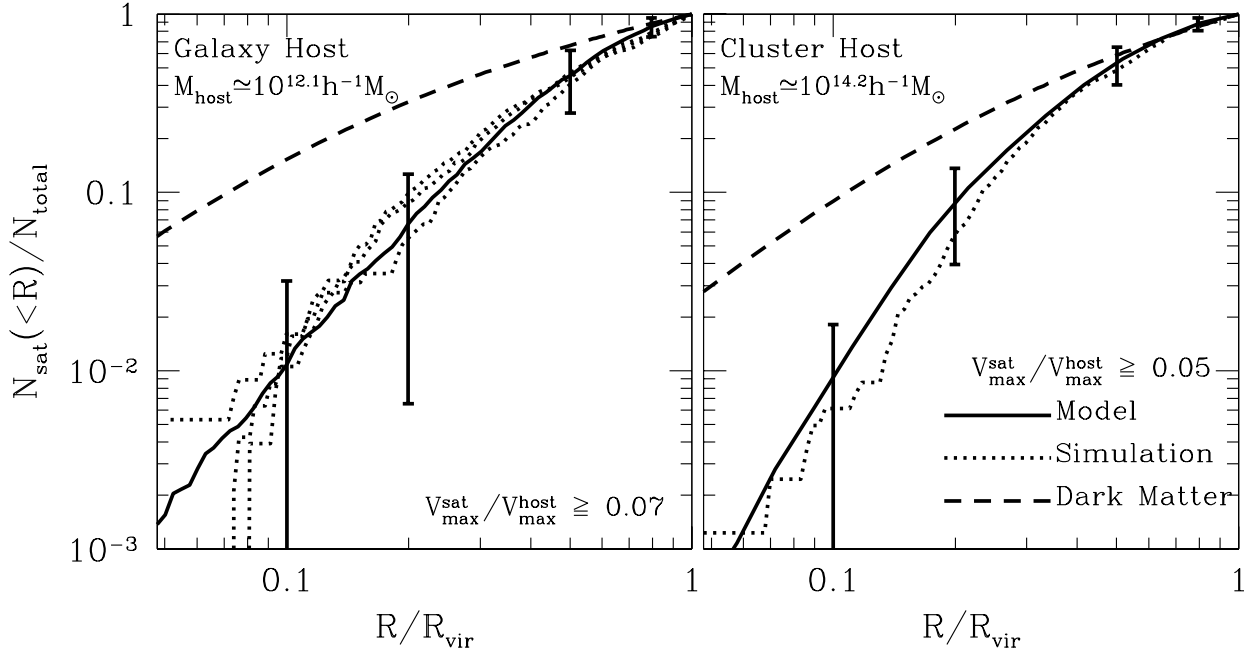


FIG. 4.— *Left Panel:* The cumulative radial distribution of satellite halos in MW-size host halos. We plot the fraction of subhalos within a given distance from the host halo center  $N_{\text{sat}}(< R)/N_{\text{total}}$  as a function of distance  $R$ , in units of the halo virial radius,  $R/R_{\text{vir}}$ . The *solid* line shows the mean cumulative radial distribution of subhalos with  $V_{\text{max}}^{\text{sat}} \geq 0.07V_{\text{max}}^{\text{host}}$  for  $M_{\text{host}} = 10^{12.1} h^{-1} M_{\odot}$  computed from 100 realizations of the semi-analytic substructure model described in § 3. The error bars show the  $1\sigma$  scatter in the 100 model realizations at only four radii for clarity. The *dotted* lines show the cumulative radial subhalo distributions for the  $G_1$ ,  $G_2$ , and  $G_3$  simulated MW-size halos. The *dashed* line represents the distribution of dark matter for an NFW halo with concentration parameter  $c_{\text{vir}} = 12.6$ , typical of a MW-size halo (B01). The simulated halos have best-fitting NFW concentrations of  $c_{\text{vir}} \simeq 9.5$ , 12.5, and 14.5. *Right Panel:* The cumulative radial distribution of satellite halos in cluster-size host halos. The line types are the same as in the *right panel*. In this case, the host mass is  $M_{\text{host}} = 10^{14.2} h^{-1} M_{\odot}$  and all subhalos with  $V_{\text{max}}^{\text{sat}} \geq 0.05V_{\text{max}}^{\text{host}}$  are plotted. The *dashed* line shows the distribution of dark matter for an NFW profile with concentration  $c_{\text{vir}} = 6.1$ , which is typical for this host mass. The best-fitting concentration for the simulated halo is  $c_{\text{vir}} \simeq 8.5$ . In both panels, the simulated radial distributions were computed by stacking the last five simulation outputs for each object.

ological model with  $\sigma_8 = 0.75$ . This power spectrum normalization is lower than the normalization of  $\sigma_8 = 0.9$  used in the simulations of the  $G_1$ ,  $G_2$ , and  $G_3$  halos as well as the CL2 cluster halo to which we compared our model in § 4.1 and § 4.2. We therefore run our model again using  $\sigma_8 = 0.75$ . The parts of the model that are directly affected by this change are the EPS merger trees of halos and their mass density profiles. Comparing the  $\Lambda\text{CDM}_{80}$  simulation results with the model at this different power spectrum normalization and at different halo masses than the  $\sigma_8 = 0.9$ ,  $M_{\text{host}} = 10^{12.1} h^{-1} M_{\odot}$  simulations that we used to tune the model is not a trivial exercise and tests the general applicability of the model.

Our first comparison is shown in Figure 5. In this plot, we show the mean number of subhalos,  $\langle N_{\text{sat}} \rangle$ , as a function of host halo mass, for four different  $V_{\text{max}}$  thresholds:  $V_{\text{max}} \geq 100$ , 150, 200, and 250  $\text{km s}^{-1}$ . The lines show the result of 1000 model realizations in each host mass bin from  $\log(M_{\text{host}}/h^{-1} M_{\odot}) = 11.0$  to  $\log(M_{\text{host}}/h^{-1} M_{\odot}) = 15.0$  with bins evenly-spaced by  $\Delta(\log M_{\text{host}}) = 0.1$ . The squares and triangles represent the  $\langle N_{\text{sat}} \rangle$  measured from the halos in the  $\Lambda\text{CDM}_{80}$  simulation.

Figure 5 shows a rather remarkable result: our model of subhalo populations matches the results of the simulations very well at each host mass and each  $V_{\text{max}}$  threshold. At a single, fixed value of  $M_{\text{host}}$ , the four model or simulation points associated with that value correspond to four

points on the CVF for host halos of that mass. As such, Figure 5 demonstrates that, after culling the input distributions for impact energies and impact parameters of subhalos at accretion from a cosmological  $N$ -body simulation of the formation of three MW-size halos, and fixing our one-parameter model to match the amplitude of the CVF of subhalos of a MW-size host, the model then successfully reproduces the CVFs of subhalos over a range of roughly three orders of magnitude in host mass in a cosmology with a different power spectrum normalization.

As a further diagnostic, we can go beyond the first moment, or mean, of the occupation distribution of subhalos and explore the shape of the probability distribution for hosting  $N_{\text{sat}}$  satellites at a given host mass  $P(N_{\text{sat}}|M_{\text{host}})$ , by comparing the second moment of the distribution. The higher order moments of the subhalo distribution are important for studies of the  $N$ -point statistics of subhalo (or galaxy) populations where  $N \geq 2$ . In Figure 6, we show results for the second moment of the subhalo occupation distribution  $\langle N_{\text{sat}}(N_{\text{sat}} - 1) \rangle$ , as a function of host mass. As in Fig. 5, the lines represent the model results, the points represent the simulation results and the error bars represent the error on  $\langle N_{\text{sat}}(N_{\text{sat}} - 1) \rangle$ . We show subhalo populations above three cuts in  $V_{\text{max}}$ , subhalos with  $V_{\text{max}} \geq 100$ , 150, 200  $\text{km s}^{-1}$ . The agreement between the model and the simulations is good for the second moment of the distribution of subhalo populations for the highest

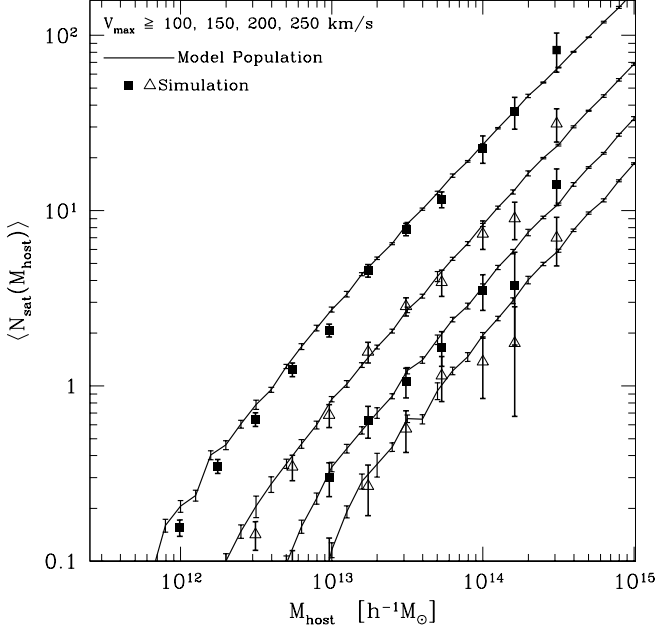


FIG. 5.— The mean subhalo occupation number as a function of host halo mass, for several peak circular velocity thresholds:  $V_{\text{max}} \geq 100, 150, 200$ , and  $250 \text{ km s}^{-1}$ . Squares and triangles show results of the  $\Lambda\text{CDM}_{80}$   $N$ -body simulation, while the results of our semi-analytic model described in § 3 is shown by the solid curves. The model results are based on 1000 Monte Carlo realizations in each host mass bin, with host mass bins spaced by  $\Delta(\log M_{\text{host}}) = 0.1$ . For both the simulation and the model results, the error bars represent the estimated error on the mean value of  $N_{\text{sat}}$  in each mass bin.

two  $V_{\text{max}}$  cuts. However, a notable feature of Fig. 6 is the discrepancy between the model results and the simulation results at low values of  $M_{\text{host}}$  or, equivalently low values of  $\langle N_{\text{sat}}(N_{\text{sat}} - 1) \rangle$ , in the lowest  $V_{\text{max}}$  sample, where the model overpredicts the second moment of the distribution by as much as  $\sim 40\%$ .

Kravtsov et al. (2004) found the second moment of the occupation distribution of subhalos to be consistent with that of a *Poisson* distribution in the host mass regime where  $\langle N_{\text{sat}} \rangle \gtrsim 0.1$ . In this case, the probability distribution function for a host halo of mass  $M_{\text{host}}$  to contain a particular number of satellite halos is completely specified by the mean of the distribution because the higher order moments are related to the mean through  $\langle N(N-1)\dots(N-i) \rangle = \langle N \rangle^{i+1}$ . In Figure 7, we compare the occupation distribution of subhalos predicted by our semi-analytic substructure model to a Poisson distribution directly by plotting the quantity

$$\alpha \equiv \langle N_{\text{sat}}(N_{\text{sat}} - 1) \rangle^{1/2} / \langle N_{\text{sat}} \rangle. \quad (9)$$

For a Poisson distribution,  $\langle N_{\text{sat}}(N_{\text{sat}} - 1) \rangle^{1/2} = \langle N_{\text{sat}} \rangle$  so that  $\alpha = 1$ , while for distributions that are narrower (*sub-Poisson*) or broader (*super-Poisson*) than a Poisson distribution,  $\alpha < 1$  and  $\alpha > 1$  respectively. Figure 7 shows  $\alpha$  as a function of  $M_{\text{host}}$  for subhalos in the semi-analytic model and the  $\Lambda\text{CDM}_{80}$  simulation for subhalos with  $V_{\text{max}} \geq 100 \text{ km s}^{-1}$ , and  $V_{\text{max}} \geq 200 \text{ km s}^{-1}$  in the left and right panels respectively. Figure 7 shows that for the  $V_{\text{max}} \geq 100 \text{ km s}^{-1}$  threshold, the semi-analytic model pro-

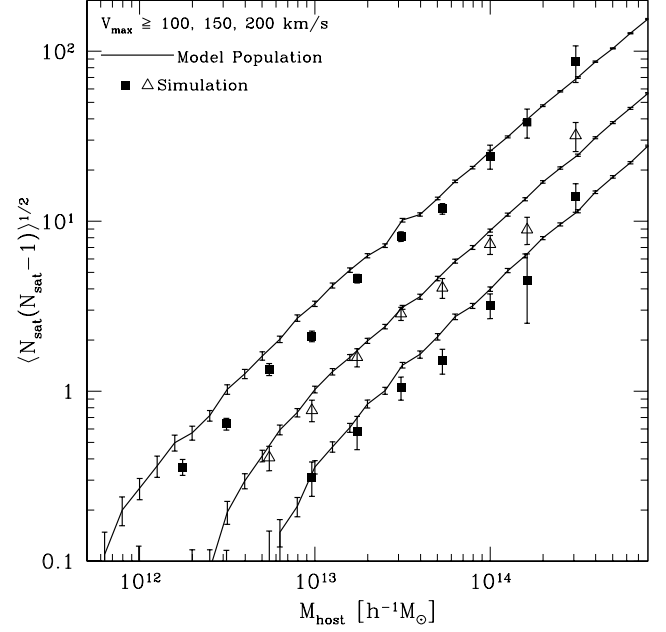


FIG. 6.— The square root of the second moment of the halo occupation distribution of subhalos  $\langle N_{\text{sat}}(N_{\text{sat}} - 1) \rangle^{1/2}$ , as a function of  $M_{\text{host}}$ . The solid lines are the mean of 1000 realizations of the semi-analytic model of § 3. The squares and triangles show the results for the subhalo populations measured in the  $\Lambda\text{CDM}_{80}$  cosmological  $N$ -body simulation. From top to bottom the three sets of lines and points are for three different subhalo  $V_{\text{max}}$  thresholds:  $V_{\text{max}} \geq 100, 150$ , and  $200 \text{ km s}^{-1}$  respectively.

duces a probability distribution for the number of satellites at a given host mass that is significantly super-Poisson in the host mass range  $10^{12} \lesssim M_{\text{host}} / h^{-1}M_{\odot} \lesssim 10^{13}$ , corresponding to a mean number of satellites  $0.1 \lesssim \langle N_{\text{sat}} \rangle \lesssim 1$ . In this range, the model over-predicts  $\alpha$  for the occupation distribution of subhalos by as much as  $\sim 25\%$  with respect to the simulated occupation distribution of subhalos. The simulated occupation distribution of subhalos is consistent with the Poisson value of  $\alpha = 1$  for  $M_{\text{host}} \gtrsim 10^{12} h^{-1}M_{\odot}$  ( $\langle N_{\text{sat}} \rangle \gtrsim 0.1$ ). At higher  $V_{\text{max}}$  thresholds, the magnitude of the discrepancy decreases, as can be seen in the right panel of Figure 7, but qualitatively, we find that the super-Poisson “bump” at  $\langle N_{\text{sat}} \rangle \sim 0.1 - 1$  persists at all  $V_{\text{max}}$  thresholds. The over-prediction of the second moment of the distribution relative to the simulation result appears to be a fairly general feature of our semi-analytic model. The model of van den Bosch et al. (2004b) yields a similar overestimate of the second moment despite the fact that their mass loss model is quite different from the model that we present, and is based on a simplified averaging of subhalo mass loss (F. C. van den Bosch, private communication). Coupling this with the fact that EPS formation times seem to exhibit a larger scatter than the formation times of simulated halos, as pointed out by W02, leads us to speculate that the origin of this discrepancy is a fundamental shortcoming of the standard EPS formalism for generating halo merger trees. Further investigation is necessary to test this hypothesis.

As a further test of the model, we generalize this comparison and examine the subhalo occupancy predicted by

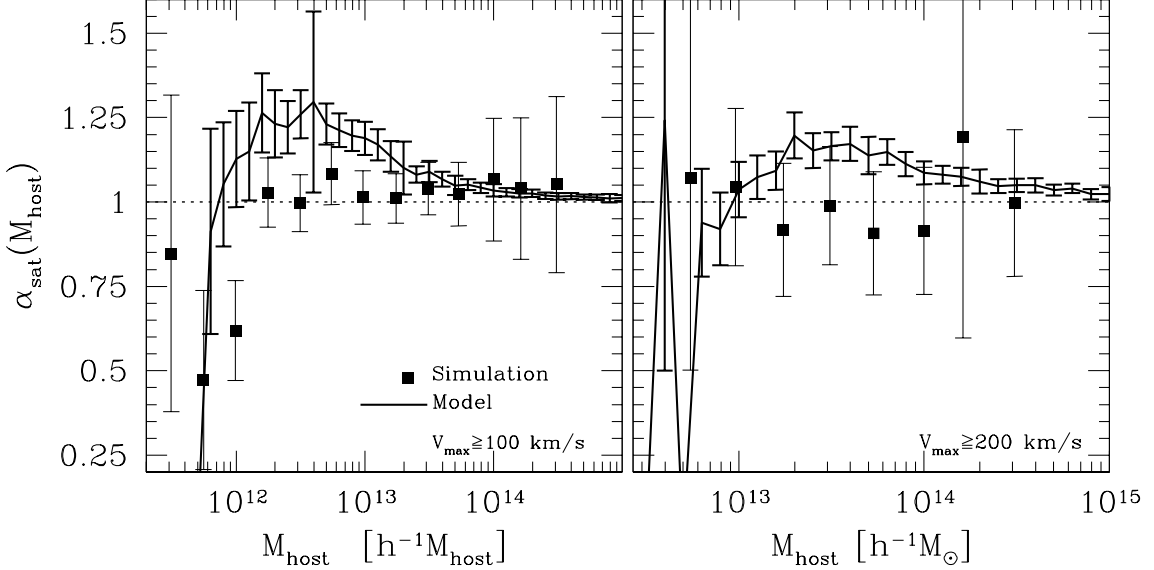


FIG. 7.— The width of the halo occupation distribution of subhalos compared to the width of the Poisson distribution. We plot the quantity  $\alpha \equiv \langle N_{\text{sat}}(N_{\text{sat}} - 1) \rangle^{1/2} / \langle N_{\text{sat}} \rangle$  as a function of host mass for two circular velocity thresholds:  $V_{\text{max}} \geq 100 \text{ km s}^{-1}$  (left panel) and  $V_{\text{max}} \geq 200 \text{ km s}^{-1}$  (right panel). The solid lines correspond to the results of the analytic model of § 3 and the squares correspond to simulation results. The horizontal dotted line marks the value  $\alpha = 1$  which corresponds to the Poisson distribution.

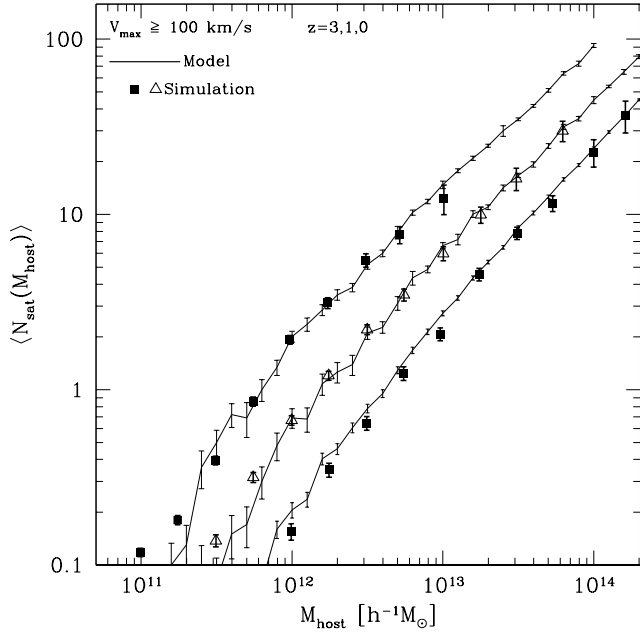


FIG. 8.— The redshift dependence of the mean of subhalo occupation. The lines show the predictions of the semi-analytic model at redshifts  $z = 0$  (bottom),  $z = 1$  (middle), and  $z = 3$  (top). The model results are based on 1000 Monte Carlo realizations at each host mass bin at  $z = 0$ , and 100 realizations at redshifts  $z = 1, 3$ . The filled squares and open triangles represent the same quantity measured from the simulations described in Kravtsov et al. (2004). For both the model predictions and the predictions of the simulations, the errorbars represent the estimated error on  $\langle N_{\text{sat}} \rangle$ . Note that we plot the subhalo occupation at only one threshold ( $V_{\text{max}} \geq 100 \text{ km s}^{-1}$ ) shown in Fig. 5 because large halos become increasingly rare with increasing redshift causing the statistics to be poor at high redshifts and large thresholds.

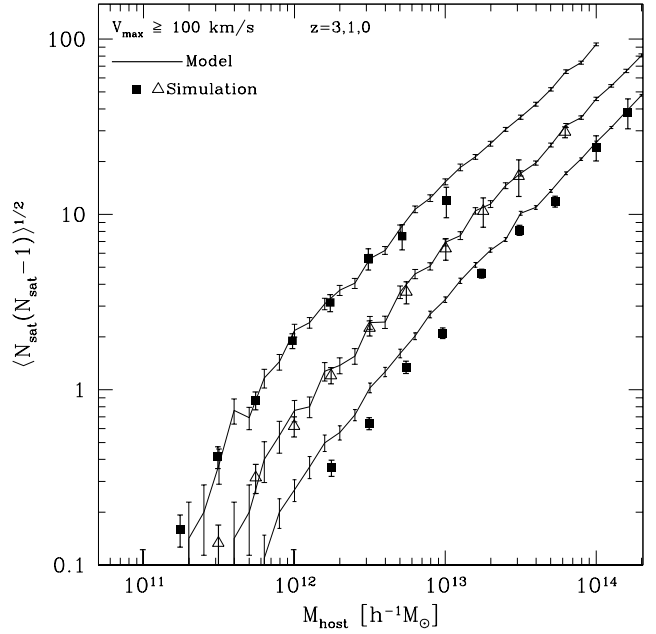


FIG. 9.— The redshift dependence of the second moment of the subhalo occupation distribution,  $\langle N_{\text{sat}}(N_{\text{sat}} - 1) \rangle^{1/2}$ . The lines show the results of the semi-analytic substructure model for subhalos with  $V_{\text{max}} \geq 100 \text{ km s}^{-1}$  at redshifts  $z = 0$  (bottom),  $z = 1$  (middle), and  $z = 3$  (top). The model results are based on 1000 model realizations at each host mass bin at  $z = 0$ , and 100 realizations at redshifts  $z = 1, 3$ . The filled squares and open triangles represent the same quantity measured from the  $\Lambda$ CDM<sub>80</sub> simulation.

the model as a function of redshift. First, Figure 8 shows the mean number of subhalos with  $V_{\text{max}} \geq 100 \text{ km s}^{-1}$  as a function of host mass at redshifts  $z = 0, 1$ , and  $3$ . We illustrate the redshift dependence using only this one  $V_{\text{max}}$

threshold at high redshift because the number of large halos decreases rapidly with redshift, causing the statistics to be rather poor at larger thresholds. At  $z = 0$  the model points represent the same 1000 realizations per mass bin as shown in Fig. 5. At redshifts  $z = 1$  and  $z = 3$ , the model results are based on 100 realizations per mass bin. Again, the agreement between the model and the  $\Lambda\text{CDM}_{80}$  simulation is rather impressive. The simple model of halo substructure that we developed in § 3, predicts a mean subhalo occupation number at high redshift that is in good agreement with the predictions of the full numerical simulation. This result also demonstrates the clear trend for CDM halos to host a larger amount of substructure at higher redshifts. Here we select halos at a fixed  $V_{\max}$  cut; using a sample selected at a fixed number density, yields the same trend, though slightly less pronounced.

The high-redshift agreement is not limited to the mean occupation. Figure 9 shows the corresponding second moment of the occupation distribution of subhalos as a function of redshift. The results are for the same model realizations used to generate Fig. 8. The figure shows that unlike at  $z = 0$ , the high redshift second moment model results are in good agreement with the  $\Lambda\text{CDM}_{80}$  simulation over a wide range of host halo masses. As redshift increases at a fixed host mass bin, the masses of the host halos in that bin become increasingly large with respect to the typical mass of collapsing objects  $M_*$ . So as redshift increases at fixed mass, we are examining increasingly rare objects. The results in Fig. 9 illustrate the same qualitative trend that is seen in Fig. 6, namely, that the model result for the second moment appears to be more like the simulation results as we examine increasingly rare host halos.

#### 4.4. Accretion vs. Destruction

Although the first detailed studies of halo substructure showed that subhalo populations may scale in a simple, nearly self-similar way with the size of the the host halo (e.g. Moore et al. 1999) there is now evidence to the contrary. Recently, Gao et al. (2004a) reported the measurement of a deviation from the self-similar scaling of subhalo populations in simulated halos (Diemand et al. 2004, hinted at this but did not have a large enough host halo sample to make a significant detection) while van den Bosch et al. (2004b) found a similar trend in subhalo abundance using analytic arguments. To be specific, Gao et al. (2004a) found that the number of subhalos with mass scaled to a fixed fraction of the host halo mass  $dN_{\text{sat}}/d(M_{\text{sat}}/M_{\text{host}})$ , increases with host mass as  $\sim M_{\text{host}}^{0.1}$  in the regime  $M_{\text{sat}}/M_{\text{host}} \ll 1$ . In Figure 3, we show that the results of our semi-analytic model predict a very similar trend with host halo mass and, as we have a large number of realizations of host halos in each mass bin, the trend that we compute is significant. Our model is in good agreement with the Gao et al. (2004a) result, yielding a subhalo abundance that scales as a power-law in the scaled satellite mass  $(M_{\text{sat}}/M_{\text{host}})$ , with a weakly host mass-dependent normalization. We find that  $dN_{\text{sat}}/d(M_{\text{sat}}/M_{\text{host}}) \propto M_{\text{host}}^\nu (M_{\text{sat}}/M_{\text{host}})^{-\mu}$  in the regime  $M_{\text{sat}}/M_{\text{host}} \ll 1$ , with  $\nu \approx 0.08$  and  $\mu \approx 1.88$ .

The semi-analytic model also provides a simple framework for understanding the nature of this trend. The abundance of subhalos is determined by the constant com-

petition between subhalo accretion and destruction. In Figure 10, we illustrate the competition between subhalo accretion and destruction rates as a function of  $M_{\text{host}}$  for different final ( $z = 0$ ) masses of the host halo. In the standard,  $\Lambda\text{CDM}$  cosmological model, the typical amplitude of mass density fluctuations is a decreasing function of length scale (or an associated mass scale  $M = 4\pi\rho_M R^3/3$  as in § 3.1), so structure forms hierarchically as small objects collapse early and merge to form larger objects. Large halos observed at redshift  $z = 0$  have thus typically assembled most of their mass relatively more recently than their less massive counterparts (e.g., see discussions in LC93 and W02). Correspondingly, one important manifestation of the more recent mass assembly of relatively massive halos is that large host halos have typically acquired their satellites more recently than less massive hosts. This shift in the relative accretion time of subhalos is evident in Fig. 10. The rate of satellite halo accretion (shown by the thick, upper lines) for the  $M_{\text{host}} = 10^{13.1} h^{-1}\text{M}_\odot$  host is strongly peaked at  $t_{\text{lookback}} \sim 10 - 11$  Gyr in the past and drops off rapidly at more recent times, while for the largest, Coma-size host, with  $M_{\text{host}} = 10^{14.6} h^{-1}\text{M}_\odot$  host, the accretion rate peaks more recently at  $t_{\text{lookback}} \sim 8 - 9$  Gyr ago and remains nearly constant from this time until the present.

The thin, lower lines in Fig. 10 show the accretion rate for *subhalos that remain above the cut  $V_{\max}^{\text{sat}} \geq 0.2V_{\max}^{\text{host}}$  at redshift  $z = 0$* . We refer to these subhalos as *surviving* subhalos. In agreement with ZB03, Gao et al. (2004a), and van den Bosch et al. (2004b), we find that only  $\sim 4 - 12\%$  of surviving subhalos are accreted prior to a redshift of  $z = 1$  ( $t_{\text{lookback}} \simeq 7.6$  Gyr). At  $t_{\text{lookback}} \sim 4$  Gyr ( $z \sim 0.35$ ), the probability of a subhalo surviving and remaining in the  $z = 0$  sample is roughly 50% and is only very weakly dependent upon the mass of the host halo. This timescale for removing subhalos from the sample due to mass loss and merging is not surprising because the typical dynamical times in halos at low redshift are of order  $\sim 3 - 5$  Gyr and lends support to the simpler approach of van den Bosch et al. (2004b) for modeling subhalo populations in applications where the level of detail we present here is not needed.

The reason for the deviation from a self-similar scaling of subhalo populations is evident in Fig. 10. Subhalos in larger hosts have typically been accreted more recently and have had less time to be tidally stripped and less time for their orbits to decay via dynamical friction and fall to the host halo center. The later formation times of more massive host halos cause the subhalo populations of host halos to deviate from self-similarity simply because the balance between typical accretion times and typical destruction times shifts monotonically in favor of accretion with increasing  $M_{\text{host}}$ . van den Bosch et al. (2004b) developed a similar interpretation of these results using an analytic model of subhalo populations.

Given the discussion of the trend in the normalization of subhalo mass and velocity functions above, it seems natural that the trend of subhalo abundance with redshift shown in Figure 8 should have a similar explanation. Along the same lines, it is also natural to inquire about subhalo survival probabilities for satellites accreted at various times. We address both of these issues in Figure 11. In the left hand panels of Fig. 11, we show the

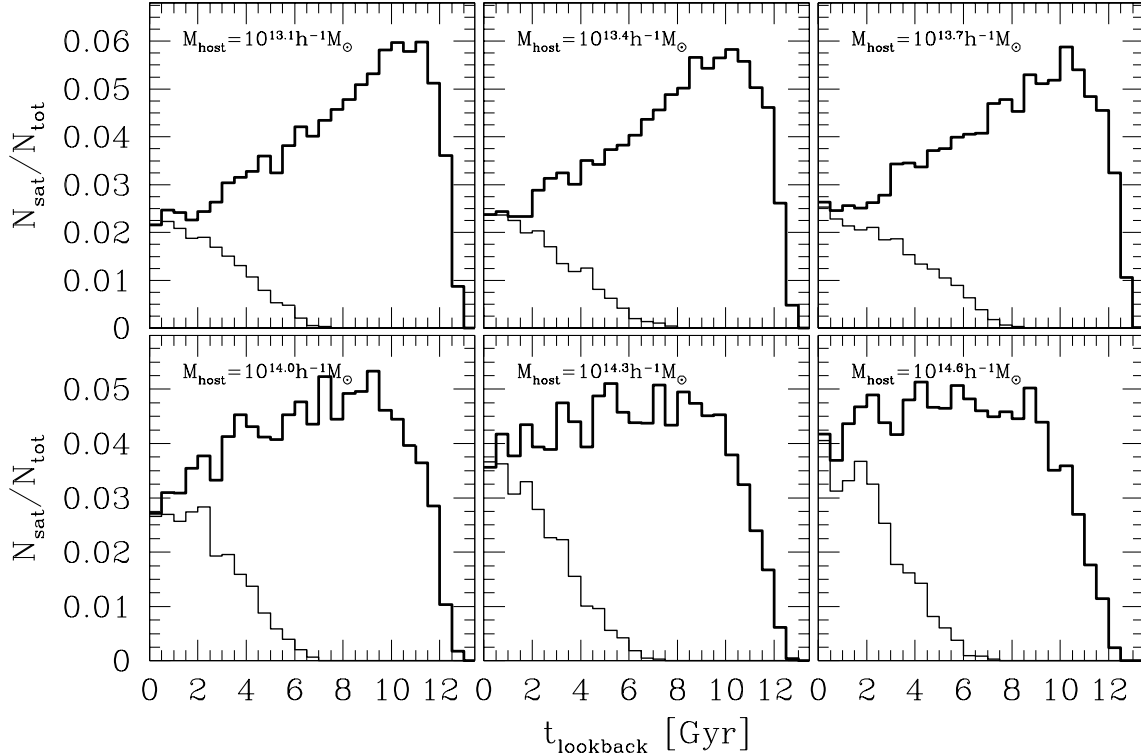


FIG. 10.— The distributions of subhalo accretion and destruction times as a function of the final  $z = 0$  host halo mass  $M_{\text{host}}$ . In each panel, we show accretion rates for the different final host masses listed in the top left of the panel. The *thick solid* upper lines indicate the number of all subhalos that are accreted with an initial maximum circular velocity  $V_{\text{max}}^{\text{sat}} \geq 0.2V_{\text{max}}^{\text{host}}$  as a function of the lookback time to the time of accretion (i.e. time *since accretion*) in bins of width  $\Delta t_{\text{lookback}} = 0.5$  Gyr. The *thin solid* lower lines show the number of subhalos accreted in each lookback time bin, which remain above the same threshold of  $V_{\text{max}}^{\text{sat}}$  at  $z = 0$ , after the various destructive effects have been accounted for. The number of subhalos in each bin is shown in units of the total number of accreted subhalos  $N_{\text{tot}}$ .

accretion rates of all subhalos (thick line) and of surviving halos (thin line) for our model realizations of host halos of mass  $M_{\text{host}} = 10^{13.5} h^{-1} M_{\odot}$  at three different redshifts,  $z = 0, 1$ , and  $3$ . In this figure, we define our subhalo samples by a fixed threshold of  $V_{\text{max}} \geq 80 \text{ km s}^{-1}$ . We refer to subhalos that remain above this threshold at the final redshift as *surviving* subhalos. We show accretion rates for halos at disparate redshifts for which the typical timescales of accretion and the typical dynamical timescales of halos are quite different from each other. In order to make the results for the halos at different redshifts more nearly commensurable, in Fig. 11 we assign subhalos an accretion time in units of the typical dynamical time of the host halo at the time of accretion  $t_{\text{lookback}}/t_{\text{dyn}}$ . The scaling of  $t_{\text{dyn}}$  with  $t_{\text{lookback}}$  is responsible for the accretion rates dropping monotonically with time, as opposed to rising, as they do in Fig. 10. In each panel, the vertical dotted line shows the median value of  $t_{\text{lookback}}/t_{\text{dyn}}$  for all accreted subhalos. The results are computed from 1000 realizations of the model of § 3.

Notice first in Fig. 11, the relative shift in the lookback time to accretion as a function of the redshift at which we observe the host halo. For the  $z = 0$  host halos, the median subhalo accretion time is roughly four halo dynamical times, while for the  $z = 3$  hosts, the median halo accretion time is only about one-half of a halo dynamical

time. The reason for this shift is essentially the same as the reason for the shift in accretion times as a function of host halo mass: large halos are increasingly rarer objects at high redshift than they are at low redshift and are characterized by more recent mass assembly.

In the right-hand panels of Fig. 11, we explicitly show the fraction of surviving subhalos  $f_{\text{surv}}$  accreted at  $t_{\text{lookback}}$ , as a function of  $t_{\text{lookback}}$  in units of the typical dynamical time of the host. In the upper right of each panel, we also show the total, integrated fraction of *all* accreted subhalos that survive until the final redshift,  $F_{\text{surv}}$ . In all cases, subhalos very rarely survive for more than  $\sim 3 - 4$  dynamical times after they are accreted onto their host halos. The typical timescale for destruction is roughly a dynamical time, as approximately 50% of all satellite halos fall below the sample  $V_{\text{max}}$  threshold after roughly one dynamical time in each case. However, notice that in the hosts observed at a final redshift of  $z = 0$ , the typical time for a subhalo to be accreted is  $\sim 3.8t_{\text{dyn}}$ , while for the host observed at  $z = 3$ , the typical subhalo accretion time is only  $\sim 0.6t_{\text{dyn}}$ . This shift in the accretion times relative to the timescale that is relevant for removing a halo from the threshold sample is dramatic and is responsible for the increase in the overall subhalo survival fraction as  $F_{\text{surv}} = 0.16, 0.22$ , and  $0.26$  for the redshifts  $z = 0, 1$ , and  $3$  halos respectively, and it is the reason

for the systematic increase in the abundance of subhalos in fixed mass hosts with increasing redshift illustrated in Fig. 8.

#### 4.5. Host Properties and Subhalo Populations

The discussion of the previous section has a natural extension. As can be seen in Fig. 2, there is a sizable scatter in the number of subhalos of a particular size in a host of *fixed* mass. In the preceding paragraphs, we demonstrated that more massive host halos typically contain more substructure simply because they assembled their mass more recently and their subunits have had less time to evolve dynamically. A natural implication of this is that the scatter in the amount of halo substructure at fixed host halo mass may be largely determined by the variety of mass accretion histories of halos at fixed mass: halos that acquired their mass more recently should have more substructure.

A convenient quantity that can be used to describe the variety of mass assembly histories of halos is the collapse epoch  $a_c$ , introduced by W02 and defined in Eq. (3) above. As we described in § 3.2, for each realization of our model, we determine the collapse epoch of the host halo by fitting Eq. (3) to its mass assembly history.

In the left panel of Figure 12, we show the correlation between  $a_c$  and satellite number predicted by our model for five different values of host mass. For each  $M_{\text{host}}$  value, we plot the number of satellites with  $V_{\text{max}}^{\text{sat}} \geq 0.15V_{\text{max}}^{\text{host}}$ , in units of the mean number of satellites for hosts of this mass, as a function of  $a_c$  in units of the mean collapse epoch  $\langle a_c \rangle$ , for hosts of this mass. The thick, solid, central line corresponds to the mean relation for  $M_{\text{host}} = 10^{14.5} h^{-1} M_\odot$  hosts and the upper and lower solid lines show the scatter in this relation measured from 1000 model realizations. The remaining lines show the mean relation between collapse epoch and satellite number for the four different host halo masses indicated in the Figure caption. The strong correlation between collapse epoch and satellite number is apparent in Fig. 12, with host halos that have an average collapse epoch hosting an average number of satellite halos. We see no evidence that this relation changes significantly as a function of host mass. Additionally, at fixed  $M_{\text{host}}$  and  $a_c$ , there remains a significant amount of scatter in the number of satellite halos, indicating that there are other important physical ingredients that affect the amount of halo substructure.

In the context of our model, two possible sources of this scatter are: (1) the distribution of orbital parameters and subhalo concentrations for a fixed host halo accretion history; (2) the variety of accretion histories that result in the same best-fit  $a_c$ . By constructing 100 model realizations using a *single* host mass accretion history in several mass bins, we estimate that approximately half of the scatter can be attributed to (1) above.

As we mentioned in § 3.2, the concentrations of halos correlate strongly with their mass accretion histories. In fact, we used this correlation to set the concentrations of our host halos according to Eq. (4), as prescribed by W02. The implication is that the fundamental correlation between mass accretion history and satellite abundance implies a correlation between host  $c_{\text{vir}}$  and  $N_{\text{sat}}$ , with  $N_{\text{sat}}$  a decreasing function of host halo concentration. In the context of our model, this correlation must be present given

the correlation between  $a_c$  and  $N_{\text{sat}}$  shown in the left panel of Fig. 12 and the fact that we assign concentrations via Eq. (4). We illustrate the model results for the  $c_{\text{vir}}-N_{\text{sat}}$  relation in the right hand panel of Fig. 12. Again, the different lines correspond to the model predictions at various host halo masses. The strong correlation between halo concentration and satellite number is clear. For this subhalo selection criterion a power-law fit to the semi-analytic model result yields  $N_{\text{sat}} \propto c_{\text{vir}}^{-a}$  with  $a \approx 0.86 \pm 0.07$ .

It is interesting to test the extent to which the simulated halos exhibit this correlation between concentration and subhalo number. The *stars* in Fig. 12 show the relationship between  $N_{\text{sat}}$  and  $c_{\text{vir}}$  for host halos in the  $\Lambda\text{CDM}_{80}$  simulation. The values for the simulation halos were computed by first selecting host halos with  $V_{\text{max}}^{\text{host}} \geq 500 \text{ km s}^{-1}$  in order to ensure the completeness of the subhalo count down to a threshold of  $V_{\text{max}}^{\text{sat}} \geq 0.15V_{\text{max}}^{\text{host}}$  (considering satellites above the scaled threshold roughly eliminates the scaling of satellite halo number with host halo size). We then fit the host density profile to an NFW profile [Eq. (2)] in order to determine the best-fit  $c_{\text{vir}}$ . Finally, we used the subhalo counts and best-fit concentrations to compute  $\langle N_{\text{sat}} \rangle$  and  $\langle c_{\text{vir}} \rangle$ . The simulated host halos also show a clear correlation between concentration and satellite number. The small number of host halos in this sample makes it difficult to draw detailed conclusions, yet the  $c_{\text{vir}}-N_{\text{sat}}$  correlation measured in the simulation appears to be in good agreement with the model predictions. This correlation also appears in agreement with the related correlation between halo  $V_{\text{max}}$  and satellite number observed in the simulations of Gao et al. (2004a). Fitting the simulated halo results to a power law  $N_{\text{sat}} \propto c_{\text{vir}}^{-a}$  yields a slightly steeper relation than the model fit, with a best-fit power-law index of  $a \approx 0.98 \pm 0.15$ . Given the errors, the power-law indices from the model and simulation data fits are consistent with each other. Interestingly, we find no statistically significant trend in the radial distribution of satellites with host halo concentration or collapse epoch.

Figure 12 shows the correlation between  $a_c$  and the number of satellite halos selected according to a specific selection threshold, namely satellites with  $V_{\text{max}}^{\text{sat}}/V_{\text{max}}^{\text{host}} \geq 0.15$ . However, we expect the strength of the correlation to be dependent upon the satellite sample threshold for several reasons. The drag of dynamical friction is proportional to  $M_{\text{sat}}^2$ , so dynamical friction is most efficient at driving rather massive satellites toward the centers of their hosts. Furthermore, the median lookback time to a merger with a satellite of a specific mass is a decreasing function of  $M_{\text{sat}}$ . Mergers with large subhalos occur relatively more recently, on average, than mergers with small subhalos. In addition, the accretion of large subhalos dominates the rate of host mass growth, so the accretion times of relatively massive subhalos more strongly influence any particular definition of formation epoch than the accretion times of small subhalos. These factors suggest that the strength of the  $a_c-N_{\text{sat}}$  (or  $c_{\text{vir}}-N_{\text{sat}}$ ) correlation should depend upon the size of the subhalos included in the sample and that the number of large subhalos should be more strongly dependent upon the mass accretion history of the host than the number of small subhalos. It is possible to use our substructure model to explore this threshold dependence, because our model provides a large number of realizations

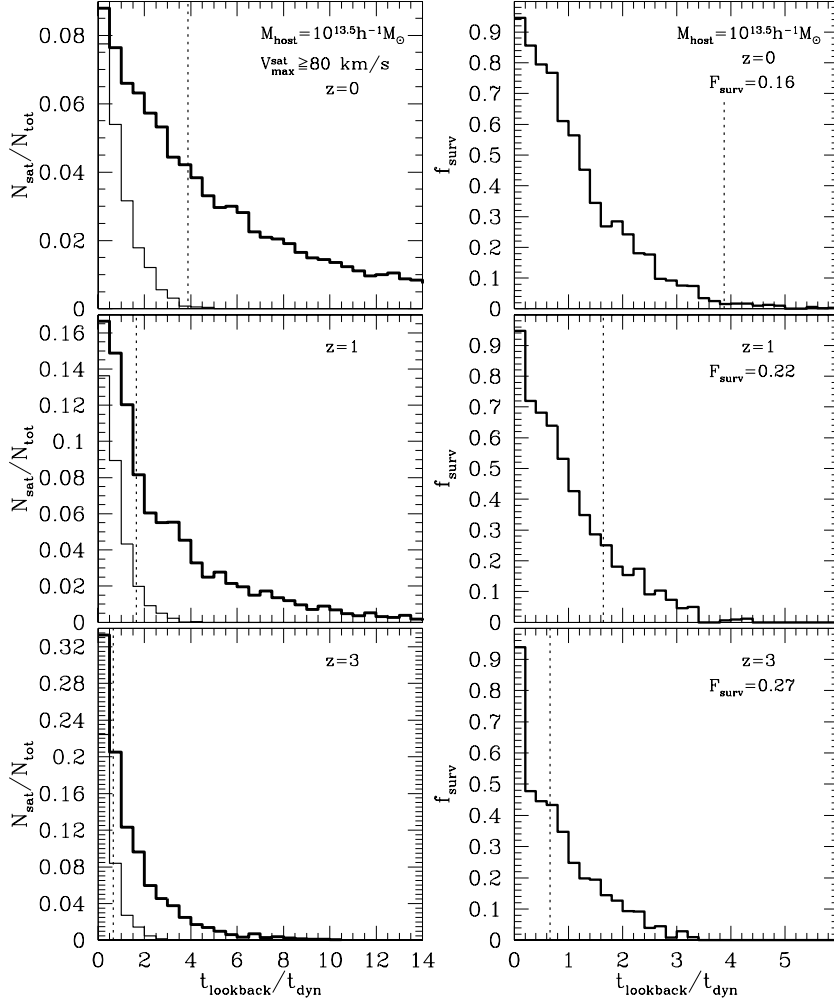


FIG. 11.— The competition between accretion and destruction at various redshifts. *Left Panels:* The *thick solid* lines show the accretion time distributions of subhalos with  $V_{\max}^{\text{sat}} \geq 80 \text{ km s}^{-1}$  at the epoch of accretion as a function of lookback time to accretion for a host of mass  $M_{\text{host}} = 10^{13.5} h^{-1} M_{\odot}$ . The lookback time has been scaled by the typical dynamical time of the host halo at the time of accretion,  $t_{\text{dyn}}$ . The *thin solid* lines show the number of accreted subhalos that remain above the aforementioned  $V_{\max}$  threshold at the redshift of observation. From top to bottom, we show the model results at final redshifts of  $z = 0, 1, 3$ . In all panels, the *vertical dotted* line depicts the median value of  $t_{\text{lookback}}/t_{\text{dyn}}$  for all accreted subhalos. *Right Panels:* The fraction of surviving subhalos as a function of the lookback time to accretion. The lines show the fraction of halos that are above the threshold  $V_{\max}^{\text{sat}} \geq 80 \text{ km s}^{-1}$  at the time of accretion and remain above this threshold at the redshift of observation. Again, the lookback time has been scaled by the dynamical time of the host halo at the time of accretion. All panels show model results for a host of mass  $M_{\text{host}} = 10^{13.5} h^{-1} M_{\odot}$  at final redshifts of (from top to bottom)  $z = 0, 1, 3$ . Listed in each panel is the total number of subhalos that are accreted with  $V_{\max}^{\text{sat}} \geq 80 \text{ km s}^{-1}$  that remain above this threshold at the redshift of observation,  $F_{\text{surv}}$ . The results shown in both panels are from 1000 realizations of the model of § 3.

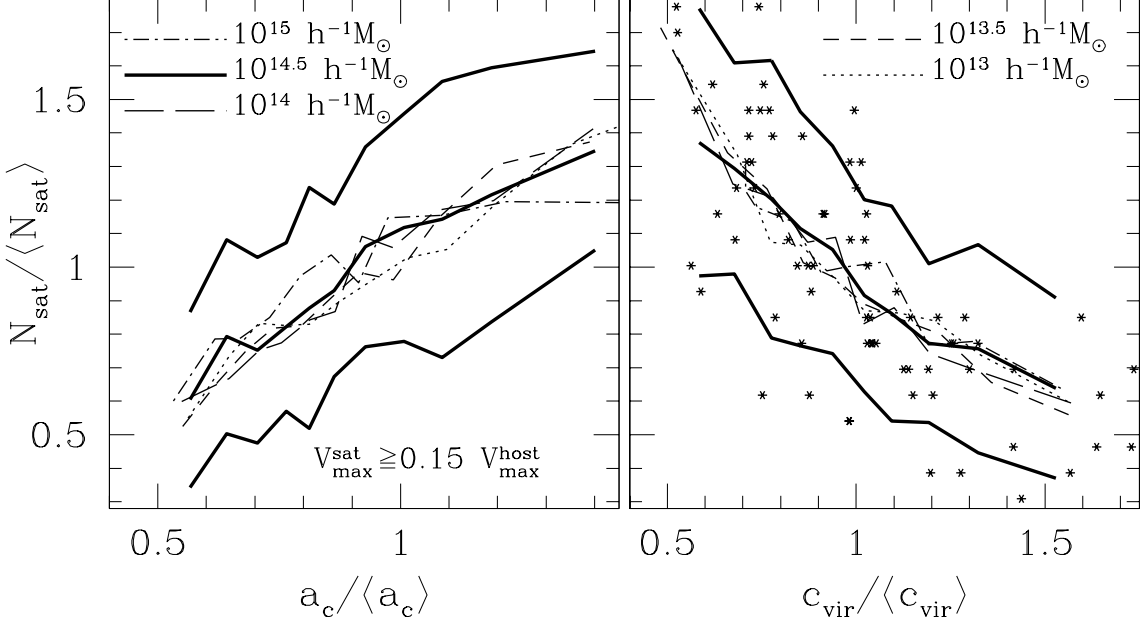


FIG. 12.— *Left Panel:* Correlation between the collapse epoch as defined in Eq. (3) and the number of surviving subhalos. We plot the mean relation between the halo collapse epoch  $a_c$ , scaled by the mean collapse epoch  $\langle a_c \rangle$ , and the number of satellites  $N_{\text{sat}}$ , scaled by the mean number of satellites  $\langle N_{\text{sat}} \rangle$ , predicted by 1000 realizations of our substructure model. The central *thick solid* line corresponds to the mean relation for  $M_{\text{host}} = 10^{14.5} h^{-1} M_{\odot}$  hosts. The other line types represent the mean relation at four different host masses:  $10^{15} h^{-1} M_{\odot}$  (*dot-dashed*),  $10^{14} h^{-1} M_{\odot}$  (*long-dashed*),  $10^{13.5} h^{-1} M_{\odot}$  (*short-dashed*), and  $10^{13} h^{-1} M_{\odot}$  (*dotted*). The upper and lower *thick, solid* lines delimit the realization-to-realization scatter in the relation based on the 1000 model realizations of a  $M_{\text{host}} = 10^{14.5} h^{-1} M_{\odot}$  host. We count only subhalos with  $V_{\text{max}}^{\text{sat}} \geq 0.15 V_{\text{max}}^{\text{host}}$  at  $z=0$ . *Right Panel:* The relationship between host halo concentration and the number of satellite halos. The lines represent the mean relation between halo  $c_{\text{vir}}$  scaled by the mean concentration  $\langle c_{\text{vir}} \rangle$ , and the number of satellite halos scaled by the mean number of satellite halos  $\langle N_{\text{sat}} \rangle$ , predicted by 1000 model realizations. The different line types correspond to different host masses and are the same as in the left panel. Again, only subhalos with  $V_{\text{max}}^{\text{sat}} \geq 0.15 V_{\text{max}}^{\text{host}}$  are counted. The stars represent the measured concentrations and satellite numbers for all host halos in the  $\Lambda$ CDM<sub>80</sub> simulation with  $V_{\text{max}}^{\text{host}} \geq 500 \text{ km s}^{-1}$ . A power-law fit to the simulation points yields  $N_{\text{sat}} \propto c_{\text{vir}}^{-a}$  with  $a \approx 0.98 \pm 0.15$ . The relationship from the subhalo model yields a slightly smaller best-fit power-law index of  $a \approx 0.86 \pm 0.07$ .

of host halos of various masses so that we are not hampered by the limited dynamic range of the cosmological simulation.

We demonstrate the  $V_{\text{max}}$  threshold dependence of the relation between  $N_{\text{sat}}$  and  $a_c$  in Figure 13. The abscissa represents minimum values of scaled maximum circular velocity  $V_{\text{max}}^{\text{sat}}/V_{\text{max}}^{\text{host}}$ , used to define various subhalo samples. At each threshold, we fit the number of satellite halos above the threshold to a power law

$$N_{\text{sat}}(> V_{\text{max}}^{\text{sat}}/V_{\text{max}}^{\text{host}}) \propto a_c^b. \quad (10)$$

At all thresholds, we find a power law to be an acceptable fit and plot the value of the best-fit power law indices on the vertical axis. The black squares show the relationship between  $b$  and  $(V_{\text{max}}^{\text{sat}}/V_{\text{max}}^{\text{host}})$  at  $z=0$ . That the strength of the correlation between satellite number and  $a_c$  is a strong function of the  $V_{\text{max}}$  threshold is evident in the Figure 13. The solid line shows the linear relation

$$b = 0.25 + 4(V_{\text{max}}^{\text{sat}}/V_{\text{max}}^{\text{host}}), \quad (11)$$

which we find to be a good fit to the relationship between the power law index  $b$ , and the sample threshold  $V_{\text{max}}^{\text{sat}}/V_{\text{max}}^{\text{host}}$ , in the regime  $0.08 \leq V_{\text{max}}^{\text{sat}}/V_{\text{max}}^{\text{host}} \leq 0.5$  at  $z=0$ . As can be seen in Fig. 13, the strength of the  $N_{\text{sat}}-a_c$  correlation declines with increasing redshift as dynamical processes become less influential in determining subhalo populations. At  $z=1$ , the best-fit relation for

the power law index is  $b \simeq 2.7(V_{\text{max}}^{\text{sat}}/V_{\text{max}}^{\text{host}})$ . The marked evolution between redshift  $z=0$  and  $z \approx 1$  is due to the cosmological constant (recall  $\Omega_{\Lambda} = 0.7$ ) which causes a dramatic reduction in the rate of structure growth, and therefore satellite accretion rates, at low redshift.

Another representation of the detailed dependence of the correlation between satellite abundance and host halo formation epoch (or host halo concentration) on the relative subhalo size is displayed in Figure 14 for cluster-size host halos. The Figure shows the differential velocity functions (DVF) of subhalos as a function  $V_{\text{max}}^{\text{sat}}/V_{\text{max}}^{\text{host}}$  for all host halos and for two subsamples subdivided by host halo formation epoch. The curves in Fig. 14 were constructed by stacking our 1000 model realizations of hosts at three masses,  $M_{\text{vir}} = 10^{14.4}$ ,  $10^{14.5}$ , and  $10^{14.6} h^{-1} M_{\odot}$ , for a total of 3000 realizations, in order to overcome noise in the measurement. The solid line represents the mean DVF for all 3000 host halos. The upper, dashed line represents the DVF for the half of the host halo sample with the highest  $a_c$  (lowest  $c_{\text{vir}}$ ), while the lower, dot-dashed line represents the DVF for the half of the sample with the lowest  $a_c$ . Again, the dependence of subhalo populations on host halo accretion history is evident. Late-forming, low concentration host halos have more substructure of all sizes and larger subhalos are more strongly correlated with accretion history and host halo  $c_{\text{vir}}$  for the aforementioned reasons. We speculate on possible implications of these

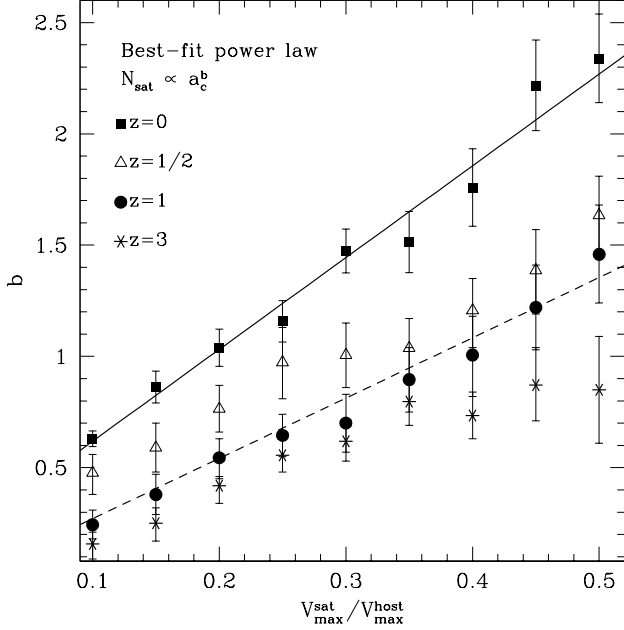


FIG. 13.— The  $N_{\text{sat}}-a_c$  relationship as a function of subhalo  $V_{\text{max}}$  threshold. We show the best-fitting power law indices from a fit of the number of satellites above a particular  $V_{\text{max}}$  threshold  $N_{\text{sat}}(>V_{\text{max}}^{\text{sat}}/V_{\text{max}}^{\text{host}})$ , to a power law function of the host halo collapse epoch  $N_{\text{sat}}(>V_{\text{max}}^{\text{sat}}/V_{\text{max}}^{\text{host}}) \propto a_c^b$ , as a function of the satellite threshold  $V_{\text{max}}^{\text{sat}}/V_{\text{max}}^{\text{host}}$  at redshifts  $z = 0$  (squares),  $z = 1/2$  (triangles),  $z = 1$  (circles), and  $z = 3$  (stars). The solid line represents a fit of the power law index  $b$ , as a function of threshold to a line,  $b \simeq 0.25 + 4(V_{\text{max}}^{\text{sat}}/V_{\text{max}}^{\text{host}})$  at  $z = 0$ . The dashed line represents a linear fit at  $z = 1$ ,  $b = 2.7(V_{\text{max}}^{\text{sat}}/V_{\text{max}}^{\text{host}})$ .

relationships in § 5.

#### 4.6. Application to Galaxy Clustering

The model that we have presented has the virtues of being simple, quick and easy to compute, easy to parse and understand, and easy to modify or add specific ingredients to. These features make the model useful for studying a wide range of phenomena. In this section, we briefly discuss the particular example of applying this model to make predictions for the two-point correlation function of galaxies. This subject will be considered in much greater detail in the subsequent papers in subsequent papers of this series.

We begin by using our model to compute the abundance of subhalos in a cosmological volume. By convolving the mean of the subhalo occupation distribution shown in Fig. 5 and Fig. 8, with the known mass function of host halos (Jenkins et al. 2001), we can compute the number density of all halos, including both host halos and their subhalos, as a function of  $V_{\text{max}}$  threshold. The result is shown in the bottom panel of Figure 15 at three redshifts:  $z = 0, 1$ , and  $3$ . The decrease in number density as a function of redshift is a reflection of the fact that fewer massive halos have collapsed at earlier epochs. The dot-dashed line in the lower panel of Fig. 15 corresponds to the mean number density of satellite halos only at  $z = 0$ . In the upper panel of Fig. 15, we show the fraction of halos that are subhalos as a function of  $V_{\text{max}}$  threshold,  $f_{\text{sat}}(>V_{\text{max}})$ . At low redshift,  $f_{\text{sat}}$  is roughly  $\sim 16 - 22\%$  at thresholds that cor-

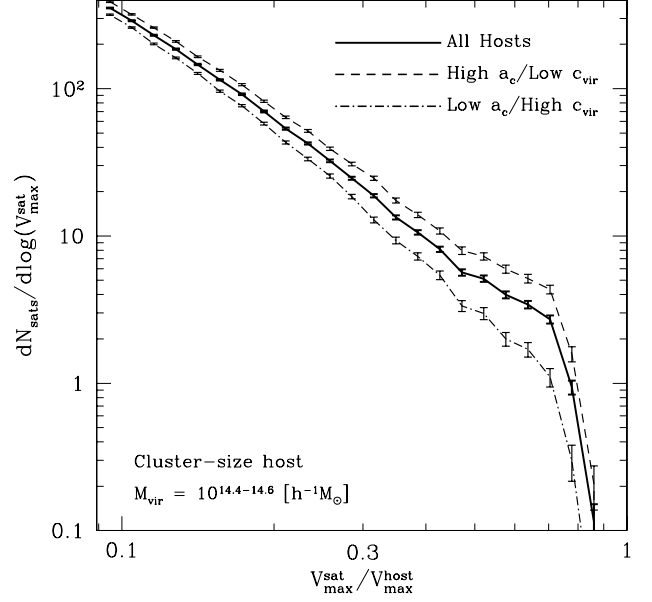


FIG. 14.— The dependence of the differential velocity function on host halo formation time and concentration. We show the differential velocity functions of subhalos in cluster-size hosts computed by stacking the 1000 model realizations in three host mass bins,  $M_{\text{vir}} = 10^{14.4}, 10^{14.5}$ , and  $10^{14.6} h^{-1} M_{\odot}$ . The thick, solid central line represents the average differential velocity function for all 3000 of the host halo realizations. The dashed line depicts the mean differential velocity function for the half of the host halo sample with the highest  $a_c$  (lowest  $c_{\text{vir}}$ ) and the lower, dot-dashed line represents the differential velocity function for the half of the host halo sample with the lowest  $a_c$  (highest  $c_{\text{vir}}$ ). In all cases, the error bars represent the estimated error on the mean value.

respond to galaxy-size halos, which is comparable to the fraction of galaxies observed to be in groups and clusters. The decrease in  $f_{\text{sat}}$  with increasing  $V_{\text{max}}$  threshold reflects the fact that the mass function of host halos  $dn/dM_{\text{host}}$ , is an increasingly steeply declining function of host halo mass. Therefore, as the threshold is increased, the number density of host halos becomes increasingly dominated by host halos near the  $V_{\text{max}}$  threshold. Halos are very unlikely to host satellites with a comparable  $V_{\text{max}}$  (see Fig. 2), so  $f_{\text{sat}}$  decreases monotonically with increasing  $V_{\text{max}}$ . A qualitatively similar argument applies to the dependence of  $f_{\text{sat}}$  on redshift at fixed  $V_{\text{max}}$ . The mass functions and the fraction of satellites are in good agreement with results of simulations presented by Kravtsov et al. (2004).

In § 1, we suggested that our model of substructure could be coupled with a low-resolution, large-volume simulation or with an analytic halo model (e.g. Seljak 2000) in order to study the clustering properties of galaxies. We pursue these applications further in the forthcoming papers of this series. However, the fact that the subhalo populations computed from our model are in good agreement with the subhalo populations of halos observed in cosmological  $N$ -body simulations does not imply that statistics that describe the spatial clustering of halos, like the two-point correlation function  $\xi(r)$ , will be in good agreement.

Consider first, populating the host halos of a low-resolution simulation with subhalo populations derived from the model of § 3. In the most common implemen-

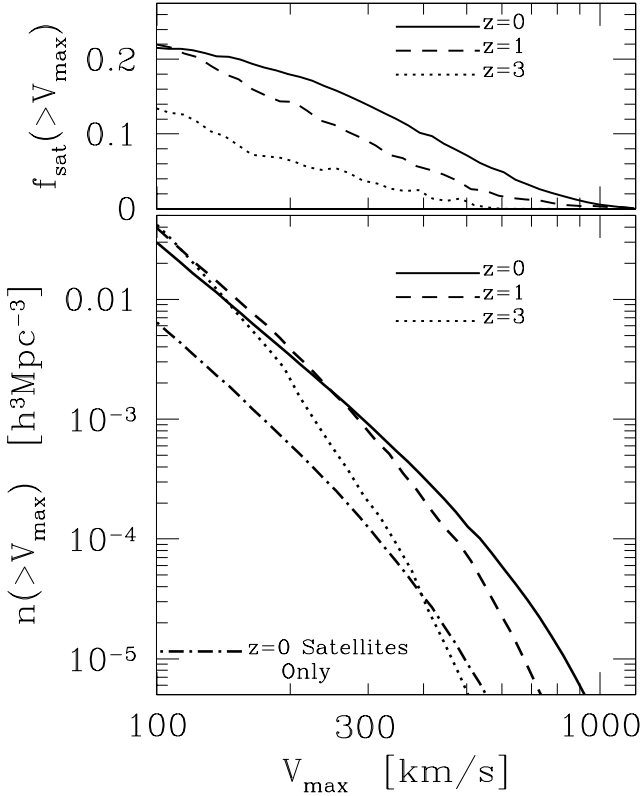


FIG. 15.— Halo and subhalo populations at three redshifts. *Bottom Panel*: The total number of halos (host halos *and* subhalos) with a maximum circular velocity greater than  $V_{\max}$  as a function of  $V_{\max}$ . The *solid* line shows the halo population at  $z = 0$ , the *dashed* line shows the halo population at  $z = 1$  and the *dotted* line shows the halo population at  $z = 3$ . The *dot-dashed* line shows the contribution from subhalos only at  $z = 0$ . *Top Panel*: The fractional contribution of subhalos to the total number of halos above each  $V_{\max}$  threshold at redshifts  $z = 0, 1, 3$ . The linetypes correspond to the same redshifts as in the *bottom* panel.

tation of the EPS formalism for hierarchical clustering (Bond et al. 1991; LC93; Somerville & Kolatt 1999), which we have used to generate mass accretion histories for our host halos, the accretion history of a halo at fixed mass is independent of its large-scale environment. There is some evidence suggesting that this practical approximation may be justified (Lemson & Kauffmann 1999; but see also Sheth & Tormen 2004). Yet, significant correlations between environment and host halo properties, such as  $a_c$  or, more generally, the entire halo mass accretion history, would also imply correlations between environment and subhalo populations. These correlations would then result in systematic differences between correlation functions measured directly from a simulated halo sample and those measured from a sample constructed by populating simulated hosts with subhalos from our model and it is important to understand this potential systematic effect before applying this method. As a byproduct, we also test the extent to which environmental effects may influence the correlation function and one of the fundamental assumptions of the halo model, the statistical independence of halo properties from halo environment.

We attempted to estimate the potential importance of these effects using the following procedure. We identified

host halos in the  $\Lambda\text{CDM}_{80}$  simulation as described in § 2, and computed their virial masses and the positions of their most bound particles. We then used these masses and positions as inputs to our substructure model. We computed a semi-analytic mass accretion history and a corresponding subhalo population for each host in the simulation, thereby constructing a hybrid catalog of simulated host halos and semi-analytic model subhalos. We reiterate that we did *not* use the concentrations or  $V_{\max}$  values of the simulated hosts in order to construct the mass accretion histories and subhalo populations. Instead, we assigned each host halo new values of  $c_{\text{vir}}$ ,  $V_{\max}$ , and  $a_c$  based on the semi-analytic mass accretion histories that we generated and the method outlined in § 3.2. As such, these host properties and the properties of their subhalos are re-assigned in a way that is independent of any effects due to the large-scale environment. However, we did use the positions of the hosts to construct our hybrid catalogs, so the hybrid catalogs exhibit the same large-scale structures as the simulation catalogs and there should thus be no differences between the two due to cosmic variance. Within each simulated host halo, we place our model subhalos at a distance  $R/R_{\text{vir}}$  from the halo’s most bound particle, where  $R/R_{\text{vir}}$  is given by the dynamical model. The subhalos are thus forced to have spherical symmetry within their hosts and do not trace the radial profiles of the N-body halos they occupy. We repeated this procedure ten times for each host halo in the  $\Lambda\text{CDM}_{80}$  simulation, thereby generating ten realizations of independent hybrid halo catalogs in order to account for variation from realization-to-realization of the semi-analytic model. Finally, we computed two-point correlation functions for the halos+subhalos in the hybrid catalogs and the  $\Lambda\text{CDM}_{80}$  simulation.

We summarize the results of this experiment in Figure 16, where we show the correlation functions for samples selected above a  $V_{\max}$  threshold of  $V_{\max} \geq 150 \text{ km s}^{-1}$ . As a reference, this threshold corresponds to a mean number density of  $n \approx 8 \times 10^{-2} h^3 \text{ Mpc}^{-3}$  (see Fig. 15), which is close to the observed number density of galaxies with  $r$ -band absolute magnitudes of  $M_r \lesssim -19.5$  (Blanton et al. 2003). The squares in Figure 16 represent the correlation function of the halos in the  $\Lambda\text{CDM}_{80}$  simulation. The error bars are the maximum of the jackknife error computed by excluding, in turn, each of the eight octants of the simulation volume and the Poisson error based on the number of pairs at each separation. A power-law fit to these points yields  $\xi(r) \simeq (r/5 \text{ } h^{-1} \text{ Mpc})^{-1.76}$ .

The shaded band shown in Fig. 16 shows the envelope of the ten correlations functions computed from our ten hybrid halo catalogs with host halo masses and positions taken from the  $\Lambda\text{CDM}_{80}$  simulation and all other halo properties, particularly the subhalo populations, determined using the semi-analytic model. The correlation functions of the halos of our hybrid model calculations are generally in remarkably good agreement with the correlation function of the simulated halos. On intermediate separations,  $r \sim 0.5 - 1 \text{ } h^{-1} \text{ Mpc}$ ,  $\xi(r)$  of the hybrid model halos is slightly higher ( $\sim 15\%$ ) than the correlation function of the  $\Lambda\text{CDM}_{80}$  halos. These separations correspond to a scale where most halo pairs are from halos that reside within the same host halo (including the host itself if it is part of the sample). In fact, the number of halo

pairs on these scales is dominated by pairs within a common host in the mass range  $10^{13} \lesssim M_{\text{host}}/h^{-1}M_{\odot} \lesssim 10^{14}$  (for example, see Berlind & Weinberg 2002). The number of pairs within a single host halo is  $N(N-1)/2$ , where  $N$  is the number of halos within the host and  $N = 1 + N_{\text{sat}}$  if the host is included in the sample while  $N = N_{\text{sat}}$  otherwise. Schematically then,  $\xi(r)$  on separations  $r \sim 0.5 - 1 h^{-1}\text{Mpc}$  is roughly set by  $\langle N(N-1) \rangle$  for hosts with  $10^{13} \lesssim M_{\text{host}}/h^{-1}M_{\odot} \lesssim 10^{14}$ . The slight enhancement of  $\xi(r)$  on these scales for the hybrid model is consistent with the differences in the second moment of the subhalo occupancy between the model results and the  $\Lambda\text{CDM}_{80}$  subhalos shown in Fig. 6.

The fact that the two-point function of the hybrid model halos is in good agreement with the two-point function of the simulated  $\Lambda\text{CDM}_{80}$  halos is encouraging. First, the properties of our hybrid model halos are independent of environment. Therefore, this calculation provides an explicit demonstration that any correlations of host halo properties, such as  $c_{\text{vir}}$ ,  $a_c$ ,  $N_{\text{sat}}(>V_{\text{max}}^{\text{sat}})$ , or the spatial distribution of subhalos within their hosts, with environment are sufficiently weak as to be nearly unmeasurable in  $\xi(r)$ . This implies that populating comparably low-resolution, large-volume simulations with subhalos from our model is a viable method for studying the two-point statistics of galaxies, though one may likely use a more sophisticated mapping of galaxies onto halos and subhalos than the simple  $V_{\text{max}}$  threshold that we used to test the importance of environmental effects. We explore such models in a forthcoming paper.

Additionally, the halo model of galaxy clustering (Neyman & Scott 1952; Scherrer & Bertschinger 1991; Seljak 2000; Scoccimarro et al. 2001) has been widely used recently for a variety of applications, one of which is to model galaxy clustering properties and to infer the galaxy occupation of dark matter halos from observational data (e.g. Zehavi et al. 2003, 2004; Zheng 2004). One of the fundamental assumptions of the halo model is that the galaxy occupation of dark matter halos is statistically independent of host halo environment and depends *only* upon  $M_{\text{host}}$ . Our results indicate that this is likely an acceptable assumption that does not lead to considerable systematic errors in  $\xi(r)$ . We close this section by illustrating the utility of our model with an explicit, entirely analytic calculation of the two point function of halos using the subhalo occupation distributions depicted in Fig. 5 and Fig. 8, coupled with the halo model. We compute the analytic correlation function as described in detail in Zehavi et al. (2004), using the host halo mass function of Jenkins et al. (2001), the dark matter correlation function of Smith et al. (2003), and the scale-dependent halo bias model of Tinker et al. (2004, in preparation). We account for the radial profile of subhalos in our model by fitting in each host mass bin, the mean radial distribution of subhalos to a profile with a constant density core:  $n_{\text{sat}}(r) \propto (1 + r/r_c)^{-3}$ . The resulting correlation function is shown as the solid line in Fig. 16. The agreement between all three methods of computing  $\xi(r)$  is apparent at all separations in the Fig. 16 and is quite impressive. The fact that the halo model calculation is lower on large scales,  $r \gtrsim 8 h^{-1}\text{Mpc}$ , is due to cosmic variance resulting from the finite size of the simulation box ( $L = 80 h^{-1}\text{Mpc}$ ).

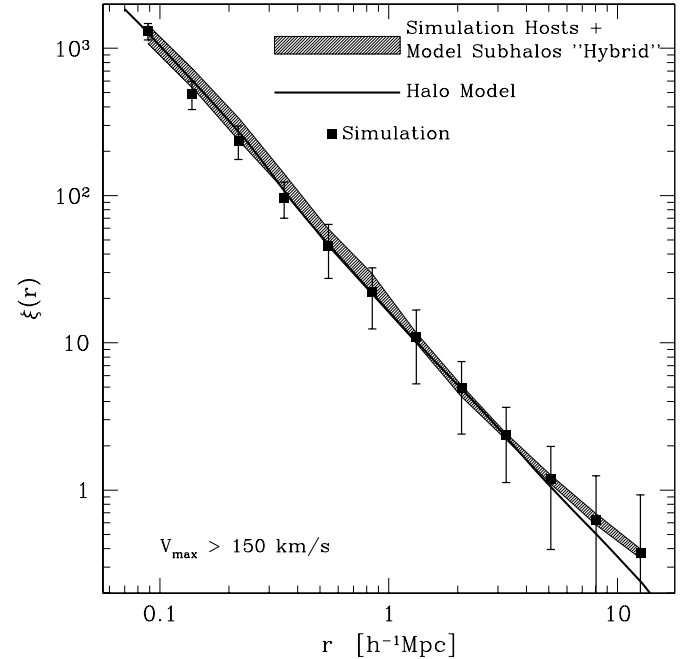


FIG. 16.— Halo two-point correlation functions for all halos (host halos and subhalos) with  $V_{\text{max}} \geq 150 \text{ km s}^{-1}$ . The *squares* represent the correlation function measured from the halos in the  $\Lambda\text{CDM}_{80}$  simulation. The error bars on the points represent the maximum of the jackknife error bars computed from the octants of the simulation box and the Poisson error based on the number of pairs. The *shaded* region represents the envelope spanned by ten realizations of our substructure model for each host halo in the simulation (see text § 4.6 for details). The *solid* line represents the correlation function computed by using the halo occupation distributions in Fig. 5 and Fig. 6, in a purely analytic computation based on the halo model of clustering.

## 5. DISCUSSION AND CONCLUSIONS

In this paper, we presented a semi-analytic model for subhalo populations within host dark matter halos. The details of the model are discussed in § 3, with some complementary information in ZB03. In the context of this model, the evolution of a subhalo population is treated as a multi-stage process and the transitions between each stage are treated as abrupt. The main ingredients of this model are as follows:

1. Semi-analytic halo merger histories, computed using the EPS formalism;
2. A method for assigning halo density profiles that incorporates the known correlations between mass accretion history and halo structure;
3. A distribution of initial orbital energies and angular momenta for merging subhalos;
4. A prescription for modeling the orbital evolution of subhalos within hosts, including the effects of orbital decay via dynamical friction and tidal mass loss.

In § 4, we make a detailed comparison between the results of our model and the results of cosmological  $N$ -body simulations in the regime where they can be compared robustly. We calibrated our one-parameter model

to match the normalization of the mean cumulative velocity function of subhalos within simulated, MW-size ( $M_{\text{host}} \approx 10^{12} h^{-1} M_{\odot}$ ) host halos at  $z = 0$ , in a standard  $\Lambda$ CDM cosmology with a power spectrum normalization of  $\sigma_8 = 0.9$ . Subsequently, we found, in the range that the simulation predictions are robust, our model to be in good agreement with the results of direct simulation. We summarize the success of our model when compared to simulation results with the following points.

1. The velocity functions of cluster-size halos in a  $\Lambda$ CDM cosmology with  $\Omega_M = 1 - \Omega_\Lambda = 0.3$ ,  $h = 0.7$ , and  $\sigma_8 = 0.9$  are in good agreement.
2. We find that the mass functions of MW-size and cluster size halos in the same,  $\Lambda$ CDM cosmology are also in agreement.
3. The model predicts a radial distribution of satellite halos within their hosts that is in good agreement with simulation results and exhibits a sizable anti-bias of subhalos with respect to the dark matter. This is in contrast to the recent results of Taylor & Babul (2004c).
4. We find a good agreement between the first and second moments of the halo occupation distribution predicted by the model and measured directly in cosmological simulations. The agreement holds for a wide range of host masses from  $M_{\text{host}} \approx 5 \times 10^{11} h^{-1} M_{\odot}$  to  $M_{\text{host}} \approx 3 \times 10^{14} h^{-1} M_{\odot}$  at redshifts  $z = 0, 1$  and  $3$  in a  $\Lambda$ CDM cosmology with a normalization of  $\sigma_8 = 0.75$ , *different* from the normalization of the simulations used to provide inputs and to calibrate the model.
5. We find a correlation between host halo collapse epoch  $a_c$ , and satellite number  $N_{\text{sat}}$ , at fixed host halo mass in our model. This implies a corresponding correlation between host  $c_{\text{vir}}$  and  $N_{\text{sat}}$  at fixed  $M_{\text{vir}}$ . We find that  $N_{\text{sat}} \propto c_{\text{vir}}^{-a}$ , with  $a \simeq 0.86 \pm 0.07$  for subhalos selected such that  $V_{\text{max}}^{\text{sat}}/V_{\text{max}}^{\text{host}} > 0.15$ . In the regime where this is testable with the simulations, we find a similar correlation. A fit to the simulation results yield a power law index  $a \simeq 0.98 \pm 0.15$ . Our model results suggest that this power law index varies rapidly with the subhalo selection criterion.
6. Our model results in deviations from a self-similar scaling of subhalo abundance with host halo mass. In particular, we find that the number of satellite halos at a fixed value of  $M_{\text{sat}}/M_{\text{host}}$  scales in proportion to  $\sim M_{\text{host}}^{0.08}$ , in approximate agreement with the recent numerical study of Gao et al. (2004a) and the analytic work of van den Bosch et al. (2004b).

The success of our model in matching the results of simulations in a variety of ways and at a variety of redshifts is non-trivial. It is also encouraging. This success suggests that such a model can be used for a wide range of applications. However, note that in contrast to our results, Taylor et al. (2003); Taylor & Babul (2004c), find that their analytic subhalo distributions are significantly more centrally concentrated than simulated subhalo populations. The two models have several different ingredients

and the root of this discord is not yet clear. Our results indicate that a centrally concentrated subhalo distribution is not a generic prediction of semi-analytic models.

We also pointed out one possible shortcoming of the model. Although the semi-analytic procedure reproduces the mean quantities observed in simulations quite well, it seems that at least over some range of host properties, the model over-predicts the second moment of the subhalo occupation  $\langle N_{\text{sat}}(N_{\text{sat}} - 1) \rangle$  when  $\langle N_{\text{sat}} \rangle$  is less than a few (see Fig. 6 and Fig. 7). The model of van den Bosch et al. (2004b) exhibits this same feature notwithstanding the fact that their treatment of mass loss is quite different from ours. We speculate that the origin of this discrepancy is a fundamental shortcoming in the standard EPS formalism for generating halo merger trees, although further work is necessary to confirm this hypothesis. W02 found that EPS merger histories have higher scatter in formation times than simulated merger histories (see also Lin, Jing, & Lin 2003); given the relation found here between  $N_{\text{sat}}$  and the formation time  $a_c$ , this discrepancy might have been anticipated.

We demonstrated explicitly, in § 4.4, that deviations in the self-similar scaling of subhalo populations with host halo mass are due to a relative shift in the balance of power between accretion rates and the orbital evolution timescales of subhalos. This argument has a natural extension. In § 4.5, we took advantage of the fact that semi-analytic approaches are not subject to the same restrictions on sample size as direct simulation, to expound upon correlations between host halo properties and their satellite populations.

We found that the host halo collapse time  $a_c$  correlates strongly with the number of satellite halos. The sense is such that early-forming halos have fewer satellites simply because they acquired their satellites earlier and these satellites were therefore subject to the destructive process of the dense, host environment for a longer time. This is in qualitative agreement with the recent, similar analysis of Taylor & Babul (2004b), who use a different definition of halo formation time. Formation time is strongly correlated with halo concentration (W02; Zhao et al. 2003), implying that satellite halo abundance is correlated with halo concentration. In our model, host halo concentration varies in inverse proportion to  $a_c$  via Eq. 4, so this correlation occurs by construction, with  $N_{\text{sat}} \propto c_{\text{vir}}^{-0.86}$  for satellites selected by  $V_{\text{max}}^{\text{sat}}/V_{\text{max}}^{\text{host}} \geq 0.15$ .

We confirmed that this correlation between halo concentration and subhalo abundance is exhibited by host halos in simulations (Fig. 12). For the  $\Lambda$ CDM<sub>80</sub> simulation, we find that  $N_{\text{sat}}(V_{\text{max}}^{\text{sat}}/V_{\text{max}}^{\text{host}} > 0.15) \propto c_{\text{vir}}^{-0.98}$ , in good agreement with the results of our model. An extension of this argument is that the strength of the  $a_c$ - $N_{\text{sat}}$  (or  $c_{\text{vir}}$ - $N_{\text{sat}}$ ) correlation should depend upon the  $V_{\text{max}}$  threshold used to define the satellite halo sample. We find that at any particular threshold of  $V_{\text{max}}^{\text{sat}}/V_{\text{max}}^{\text{host}}$ ,  $N_{\text{sat}} \propto a_c^b$ , where  $b \simeq 0.25 + 4(V_{\text{max}}^{\text{sat}}/V_{\text{max}}^{\text{host}})$ , for  $0.08 \leq V_{\text{max}}^{\text{sat}}/V_{\text{max}}^{\text{host}} \leq 0.5$  at redshift  $z = 0$ . We find that the correlation between formation time and satellite abundance (or, equivalently, between host concentration and satellite abundance) becomes weaker at high redshift as shown in Fig. 13. By redshift  $z = 1$ , the relation between the number of satellites and the host halo formation time is described by a

power law index  $b \simeq 2.7(V_{\max}^{\text{sat}}/V_{\max}^{\text{host}})$ .

These results may have direct observational implications. For example, cluster halos of fixed mass but with below average substructure counts are objects that acquired their substructure earlier, allowing satellites to experience significant dynamical evolution. If accretion into a cluster environment strips gas from the subhalo and effectively truncates star formation, this suggests that these early-forming clusters may have a higher fraction of red galaxies. More directly, in a sample of clusters restricted about a narrow range of X-ray temperatures or luminosities, cluster richness may be expected to correlate with the fraction of red galaxies.

Similarly, central galaxy mergers would be more common in these early-forming systems, likely causing the central galaxy to become more luminous. This may induce a correlation between cluster richness and the luminosity of the brightest cluster galaxy in systems of fixed dynamical mass. We are tempted to identify the so-called *fossil groups* with the extreme, early-formation tail of the formation epoch ( $a_c$ ) distribution in our model. The fossil groups are systems that are characterized by X-ray luminosities comparable to those of poor galaxy clusters, while their optical luminosities are dominated by a single, bright, central galaxy (e.g., Vikhlinin et al. 1999; Jones et al. 2003). In this scenario, these fossil groups would correspond to large, group-size halos that assembled their mass very early, when dynamical timescales were short, allowing any substructure to evolve significantly. Any large satellites would then be more vulnerable to a rapid merger with the central object due to dynamical friction, leaving a luminous central galaxy, and to severe tidal disruption, leaving a surrounding halo bereft of luminous companions. This interpretation is consistent with the analyses of the radial distribution of low-luminosity satellite galaxies in such groups (Mathews et al. 2004).

The correlation between  $N_{\text{sat}}$  and  $c_{\text{vir}}$  may be detectable observationally. Our results suggest that for clusters with similar mass estimates, the optically-richer clusters should have underlying dark matter halos with concentrations that are lower than average. It may be possible to detect directly trends of this kind using cluster mass profile estimates either via X-ray analyses or gravitational lensing. If a trend between formation time or concentration and the number of satellite galaxies  $N_{\text{gal}}$ , could be detected using optical data, it could potentially provide an optical mass measurement with less scatter than  $N_{\text{gal}}$  or total cluster luminosity. Specifically, a large fraction of the scatter in mass at a fixed observed value of  $N_{\text{gal}}$  in the newest generation of optically-selected cluster catalogs is due to the theoretically-expected scatter in  $N_{\text{gal}}$  at fixed mass (R. H. Wechsler et al., in preparation). The aforementioned correlation suggests that clusters at fixed  $N_{\text{gal}}$  are a mix of later-forming, low-mass clusters and earlier-forming, high-mass clusters. Thus, it may be possible to remove some of this scatter with other optical observables.

Finally, we demonstrated the utility of the presented model with an explicit calculation of correlation functions in § 4.6. We generated a set of ten hybrid halo catalogs using the host halos from the  $\Lambda\text{CDM}_{80}$  simulation and ten semi-analytically computed subhalo populations for each host. We computed the two-point correlation function of

the  $\Lambda\text{CDM}_{80}$  halos and compared it with the correlation functions of the halos in the hybrid catalogs. We found the correlation functions calculated in this way to be in good agreement. The host concentrations and the hybrid model subhalos are assigned according to a technique that is ignorant of the environment of the halo. This result implies that any correlations between  $c_{\text{vir}}$ ,  $N_{\text{sat}}(> V_{\max}^{\text{sat}})$ , or subhalo spatial distributions with environment are sufficiently weak that they likely do not have a measurable effect on the correlation function. This supports one of the basic assumptions of halo model analysis of galaxy clustering (e.g. Zehavi et al. 2003, 2004), namely that the galaxy occupation of host halos is statistically independent of environment and depends solely upon the mass of the halo. This also suggests that the technique of populating a large-volume, low-resolution simulation with semi-analytic subhalo populations is viable for studying galaxy clustering and environment. We pursue these issues in a forthcoming paper in which we also study mapping galaxies onto halos using various prescriptions in order to test several hypotheses about the physics of galaxy formation.

We thank Avishai Dekel, Q. Y. Gong, Stelios Kazantzidis, Savvas Koushiappas, Rachel Somerville, James Taylor, and Jeremy Tinker for useful discussions and feedback. We thank Neal Dalal, Stelios Kazantzidis, Roman Scoccimarro, Frank van den Bosch, David Weinberg, and Zheng Zheng for valuable comments on an earlier draft of this manuscript and several helpful suggestions. This research made use of the NASA Astrophysics Data System. ARZ would like to thank the Center for Cosmology and Particle Physics at New York University for its hospitality during several visits while this work was in progress and the 2004 Santa Fe Cosmology Workshop where part of this work was completed. This work was partially funded by The Kavli Institute for Cosmological Physics at The University of Chicago and the National Science Foundation (NSF) through grant No. NSF PHY 0114422. AAB is partially supported by NASA (grant NAG5-11669) and NSF (grant PHY-0101738). AVK is supported by the NSF under grants No. AST-0206216 and AST-0239759, by NASA through grant NAG5-13274, and by the Kavli Institute for Cosmological Physics at the University of Chicago. RHW is supported by NASA through a Hubble Fellowship awarded by the Space Telescope Science Institute, which is operated by the Association of Universities for Research in Astronomy, Inc., for NASA, under contract NAS 5-26555. The simulations used in this study were performed on the IBM RS/6000 SP3 system at the National Energy Research Scientific Computing Center (NERSC).

## REFERENCES

- Benson, A. J., Lacey, C. G., Baugh, C. M., Cole, S., & Frenk, C. S. 2002, MNRAS, 333, 156
- Benson, A. J. 2004, MNRAS, submitted, (astro-ph/0407428)
- Berlind, A. A., & Weinberg, D. H. 2002, ApJ, 575, 587 (BW)
- Blanton, M. R. et al. 2003, ApJ, 592, 819
- Binney, J. J. & Tremaine, S. 1987, Galactic Dynamics, (Princeton:Princeton University Press)
- Bond, J. R., Cole, S., Efstathiou, G., & Kaiser, N. 1991, ApJ, 379, 440

- Blumenthal, G. R., Faber, S. M., Primack, J. R., & Rees, M. J. 1984, *Nature*, 311, 517
- Bradač, M., Schneider, P., Steinmetz, M., Lombardi, M., King, L. J., & Porcas, R. 2002, *A&A*, 388, 373
- Bryan, G. L. & Norman, M. L. 1998, *ApJ*, 495, 80
- Bullock, J. S., Kravtsov, A. V., & Weinberg, D. H. 2000, *ApJ*, 539, 517
- Bullock, J. S., Kravtsov, A. V., & Weinberg, D. H. 2001a, *ApJ*, 548, 33
- Bullock, J. S., Kolatt, T. S., Sigad, Y., Somerville, R. S., Kravtsov, A. V., Klypin, A. A., Primack, J. R., & Dekel, A. 2001, *MNRAS*, 321, 559 (B01)
- Carlberg, R. G., Yee, H. K. C., & Ellingson, E. 1997, *ApJ*, 478, 462
- Chandrasekhar, S. 1943, *ApJ*, 97, 255
- Chen, J., Kravtsov, A. V., & Keeton, C. R. 2003, *ApJ*, 592, 24
- Cole, S., Lacey, C., Baugh, C. M., & Frenk, C. S. 2000, *MNRAS*, 319, 168
- Cole, S. et al. 2001, *MNRAS*, 326, 255
- Colín, P., Klypin, A. A., Kravtsov, A. V., & Khokhlov, A. 1999, *ApJ*, 523, 32
- Colless, M. et al. 2001, *MNRAS*, 328, 1039
- Colpi, M., Mayer, L., & Governato, F. 1999, *ApJ*, 525, 720
- Dalal, N. & Kochanek, C. S. 2001, *ApJ*, 572, 25
- Diemand, J., Moore, B., & Stadel, J. 2004, *MNRAS*, 352, 535
- Eke, V. R., Navarro, J. F., & Frenk, C. S. 1998, *ApJ*, 503, 569
- Gao, L., White, S. D. M., Jenkins, A., Stoehr, F., & Springel, V. 2004a, *MNRAS*, accepted
- Gao, L., De Lucia, G., White, S. D. M., & Jenkins, A. 2004b, *MNRAS*, 352, L1
- Ghigna, S., Moore, B., Governato, F., & Stadel, J. 1998, *MNRAS*, 300, 146
- Ghigna, S., Moore, B., Governato, F., Lake, G., Quinn, T., & Stadel, J. 2000, *ApJ*, 544 616
- Hashimoto, Y., Funato, Y. & Makino, J. 2003, *ApJ*, 582, 196
- Hayashi, E., Navarro, J. F., Taylor, J. E., Stadel, J., & Quinn, T. 2003, *ApJ*, 584, 541
- Islam, R. R., Taylor, J. E., and Silk, J. 2003, *MNRAS*, submitted
- Jenkins, A., Frenk, C. S., White, S. D. M., Colberg, J. M., Cole, S., Evrard, A. E., Couchman, H. M. P., Yoshida, N. 2001, *MNRAS*, 321, 372
- Jing, Y. P. 1998, *ApJ*, 503, L9
- Johnston, K. V. 1998, *ApJ*, 495, 297
- Jones, L. R., Ponman, T. J., Horton, A., Babul, A., Ebeling, H., Burke, D. J. 2003, *MNRAS*, 343, 627
- Kazantzidis, S., Magorrian, J., & Moore, B. 2004, *ApJ*, 601, 37
- Kazantzidis, S., Mayer, L., Mastroberto, C., Diemand, J., Stadel, J., & Moore, B. 2004, *ApJ*, 608, 663
- King, I. 1962, *AJ*, 67, 471
- Klypin, A. A., Kravtsov, A. V., Valenzuela, O., & Prada, F. 1999a, *ApJ*, 522, 82
- Klypin, A. A., Gottlöber, S., Kravtsov, A. V., & Khokhlov, A. M. 1999b, *ApJ*, 516, 530
- Klypin, A. A., Kravtsov, A. V., Bullock, J. S., & Primack, J. R. 2001, *ApJ*, 554, 903 (K01)
- Koushiappas, S. M., Zentner, A. R., & Walker, T. P. 2004, *Phys. Rev. D*, 69, 043501
- Kravtsov, A. V., Klypin, A. A., & Khokhlov, A. M. 1997, *ApJS*, 111, 73
- Kravtsov, A. V. 1999, Ph.D. Thesis, New Mexico State University
- Kravtsov, A. V., & Klypin, A. A. 1999, *ApJ*, 520, 437
- Kravtsov, A. V., Berlind, A. A., Wechsler, R. H., Klypin, A. A., Gottlöber, S., Allgood, B., & Primack, J. R. 2004, *ApJ*, 609, 35
- Kravtsov, A. V., Gnedin, O. Y., & Klypin, A. A. 2004, *ApJ*, 609, 482 (KGK04)
- Lacey, C. & Cole, S. 1993, *MNRAS*, 262, 627 (LC93)
- Lacey, C. G., & Cole, S. 1994, *MNRAS*, 271, 676
- Lemson, G. & Kauffmann, G. 1999, *MNRAS*, 302, 111
- Lin, W. P., Jing, Y. P., & Lin, L. 2003, *MNRAS*, 344, 1327
- Lin, Y., Mohr, J. J., & Stanford, S. 2004, *ApJ*, 610, 745
- Mathews, W. G., Chomiuk, L., Brighenti, F. & Buote, D. A. 2004, *ApJ*, submitted (astro-ph/0408144)
- Mayer, L., Moore, B., Quinn, T., Governato, F., & Stadel, J. 2002, *MNRAS*, 336, 119
- Mo, H. J. & White, S. D. M. 1996, *MNRAS*, 282, 347
- Moore, B., Ghigna, S., Governato, F., Lake, G., Quinn, T., Stadel, J., & Tozzi, P. 1999, *ApJ*, 524, L9
- Nagai, D. & Kravtsov, A. V. 2005, *ApJ*, in press (astro-ph/0408273)
- Neyman, J. & Scott, E. L. 1952, *ApJ*, 116, 144
- Neyrinck, M. C., Hamilton, A. J. S., & Gnedin, N. Y. 2004, *MNRAS*, 348, 1
- Navarro, J. F., Frenk, C. S., & White, S. D. M. 1997, *ApJ*, 490, 493 (NFW)
- Oguri, M. & Lee, J. 2004, *MNRAS*, in press (astro-ph/0401628)
- Reed, D., Governato, F., Quinn, T., Gardner, J., Stadel, J., & Lake, G. 2004, *MNRAS*, submitted (astro-ph/0406034)
- Scherrer, R. J. & Bertschinger, E. 1991, *ApJ*, 381, 349
- Scoccimarro, R., Sheth, R. K., Hui, L., & Jain, B. 2001, *ApJ*, 546, 20
- Seljak, U. 2000, *MNRAS*, 318, 203
- Seljak, U. & Warren, M. 2004, *MNRAS*, submitted
- Sheth, R. K. & Lemson, G. 1999, *MNRAS*, 305, 946
- Sheth, R. K., Mo, H. J., & Tormen, G. 1999, *MNRAS*, 323, 1
- Sheth, R. K., Diaferio, A., Hui, L., & Scoccimarro, R. 2001, *MNRAS*, 326, 463
- Sheth, R. K., Tormen, G. 2004, *MNRAS*, 350, 1385
- Smith, R. E. et al. 2003, *MNRAS*, 341, 1311
- Somerville, R. S. & Kolatt, T. S. 1999, *MNRAS*, 305, 1
- Springel, V., White, S. D. M., Tormen, G., & Kauffmann, G. 2001, *MNRAS*, 328, 726
- Taffoni, G., Mayer, L., Colpi, M., & Governato, F. 2003, *MNRAS*, 341, 434
- Tasitsiomi, A., Kravtsov, A. V., Gottlöber, S., & Klypin, A. A. 2004, *ApJ*, 607, 125
- Taylor, J. E., & Babul, A. 2001, *ApJ*, 559, 716
- Taylor, J. E., Silk, J., & Babul, A. 2003, in IAU Symposium (astro-ph/0312086)
- Taylor, J. E., & Babul, A. 2004a, *MNRAS*, 348, 811
- Taylor, J. E., & Babul, A. 2004b, *MNRAS*, submitted (astro-ph/0410048)
- Taylor, J. E. & Babul, A. 2004c, *MNRAS*, submitted (astro-ph/0410049)
- van den Bosch, F. C., Yang, X., Mo, H. J., and Norberg, P. 2004a, *MNRAS*, submitted (astro-ph/0406246)
- van den Bosch, F. C., Tormen, G., & Giocoli, C. 2004b, *MNRAS*, submitted (astro-ph/0409201)
- van der Marel, R. P., Magorrian, J., Carlberg, R. G., Yee, H. K. C. & Ellingson, E. 2000, *AJ*, 119, 2038
- Velázquez, H. & White, S. D. M. 1999, *MNRAS*, 304, 254
- Vikhlinin, A., McNamara, B. R., Hornstrup, A., Quintana, H., Forman, W., Jones, C., Way, M. 1999, *ApJ*, 520, L1
- Wechsler, R. H., Bullock, J. S., Primack, J. R., Kravtsov, A. V., & Dekel, A. 2002, *ApJ*, 568, 52 (W02)
- White, S. D. M. 1976, *MNRAS*, 174, 467
- White, S. D. M. & Rees, M. J. 1978, *MNRAS*, 183, 341
- White, S. D. M. 1996, in *Cosmology and Large-Scale Structure*, ed. R. Schaeffer, J. Silk, & J. Zinn-Justin (Dordrecht: Elsevier Science)
- Zhao, D. H., Mo, H. J., Ying, Y. P., and Börner, G. 2003, *MNRAS*, 339, 12
- Zehavi, I. et al. 2002, *ApJ*, 571, 172
- Zehavi, I. et al. 2003, *ApJ*, in press (astro-ph/0301280)
- Zehavi, I. et al. 2004, *ApJ*, submitted (astro-ph/0408569)
- Zentner, A. R., & Bullock, J. S. 2003, *ApJ*, 598, 49 (ZB03)
- Zheng, Z. 2004, *ApJ*, 610, 61